Determining uranium activity distribution in water streams and sediment in three mining regions of South Africa

P Mashamaite

orcid.org/0000-0002-7987-1321

Mini-Dissertation accepted in partial fulfillment of the requirements for the degree Master of Science in Applied Radiation Science at the North West University

Supervisor: Prof M Mathuthu

Graduation: July 2023

Student number: 33677352

Declaration

I, Phuti Mashamaite (student number 33677352), hereby declare that this dissertation represents my individual research and all contributions from external sources have been accurately identified with appropriate citations to the literature and acknowledgement of the research and discussions. It is being submitted for the degree of Master of Science at the North-West University. It has not been submitted before for any degree or examination at any other University.

Dedication

To my parents for their never-ending support and limitless supply of all I need.

Acknowledgements

I take this opportunity to express gratitude to all my supervisors, named and unnamed on this paper, for their support and guidance in carrying out this project. Secondly, I thank the Centre for Applied Radiation Science and Technology (CARST) staff, who supported me throughout my studies. Thirdly, many thanks to all my colleagues from the South African National Nuclear Regulator for their assistance and responses to all my requests. Lastly, I thank my fellow post-graduates, specifically Ms. Ontlametse Nkgwang, with whom I have been exchanging words of encouragement and keeping each other awake during late nights and weekend study sessions.

Abstract

Uranium is a by-product in the mining of gold in South African landscapes (Coetzee et al., 2006). Since these activities are done on land in different provinces of South Africa and near communities inhabited by people and animals, there is a risk of exposure from this uranium by-product during operations and after operations have ceased. It is therefore necessary to determine the levels of contamination at present to identify the potential risks posed to people and the environment. The purpose of this study was to determine the activity concentrations of uranium isotopes (^{238}U, ^{235}U, and ^{234}U) in sediment and water and the $^{234}U/^{238}U$ activity ratios in the water around gold mining operations in Gauteng, North West, Free State, and Mpumalanga province. The concentration of uranium in water and sediment around the Witwatersrand Basin covering the mining regions of Gauteng (West Rand location), the North West (Klerksdorp location), the Free State (Welkom location), and Mpumalanga (East Rand location) provinces in South Africa was determined using alpha spectrometry and gamma spectrometry. Water and sediment samples were collected during different months of the year in these regions. The selected months were times when different seasons of the year started, i.e., September (the beginning of Spring), December (the beginning of Summer) and March (the beginning of Autumn). This selection was made to see whether the change in the season impacted the activity concentration levels. The samples were contained in plastic bottles and tubs and then transported to the laboratory for analysis. Alpha spectrometry was used to analyse water samples, and Gamma spectrometry was used to analyse sediment samples to determine the activity concentration of uranium and the concentration of uranium in water and sediment. The transfer coefficient of uranium in water was calculated from the concentration results. The highest uranium concentration in water and sediment was found in West Rand. The concentration in water and sediment, respectively, had a mean value of 7263,8 mBq/L and 1871,7 Bq/kg in West Rand; 2346 mBq/L and 186,7 Bq/kg in Welkom; 1887,7 mBq/L and 452,2 Bq/kg in Klerksdorp and 807,2 mBq/L and 260 Bq/kg in East Rand. The isotopic ratios of $^{234}U/^{238}U$ for all the samples collected ranged from 0,96 to 1,14. The resultant values in this study indicated that ^{238}U activity concentration is significant throughout the spring, summer, and autumn seasons. Some values exceeded 500 Bq/kg, which is the National Nuclear

Regulator’s limit for exclusion of operations. Some low values observed during the December 2020 period could be due to the rainfall during that time.

Keywords

Uranium; Activity concentration; Radioisotopes; Sediment, Water streams; Gama spectrometry; Alpha spectrometry.

Table of Contents

List of figures

List of tables

List of Abbreviations

Ca – Calabrian arc

CARST – Centre for Applied Radiation Science and Technology

DNA – Deoxyribonuclease acid

FWHM – Full Width at Half Maximum

Ga – Giga annum

HPGe – High Purity Germanium Detector

ICP-MS – Inductively Coupled Plasma Mass Spectrometry

keV – Kilo-electron volts

Km – kilo metres

LabSOCS – Laboratory Sourceless Calibration Software

Ma – Meso archaean

MeV – Mega electron volts

NaI(Tl) – Thalium-activated Sodium Iodide

NIST – National institute of standards and technology

NNR – National Nuclear Regulator

NORMs – Naturally Occurring Radioactive Materials

Ppm – Parts per million

U – Uranium

UTEVA – Uranium and Tetra valent Actinides

Chapter 1: Introduction and Problem statement

1.1 Introduction

The discovery of gold in South Africa was first recorded in 1886 in Witwatersrand (Durand, 2012; Papanicolaou et al., 2010). After this discovery, gold became a driving force of the South African economy, and the country grew to be one of the largest gold producers in the world. More gold mines started to operate across the country over time. Gold mining in South Africa has been rising since the nineteenth century (Marais & Nel, 2016). Mining cuts across different provinces, including Gauteng, the North West, and the Free State. The Witwatersrand Basin, which covers all three provinces, has produced 40% of the gold ever mined and still has over a third of unmined reserves in the world (Frimmel & Minter, 2002). The basin is situated on the Kaapvaal Crayton, formed during the Archaean. The basin lies above a basement composed of greenstone belts, granitoid and Calabrian arc (ca) 3.1 Giga annum (Ga) or 1-billion-year-old volcanics and sediments of the dominion group. Above the basement is the Witwatersrand Supergroup, which comprises the West Rand, which contains sandstones and foredeep shales, and Central Rand, comprising alluvial sandstones and auriferous conglomerates as shown in figure 1.1 (Jolley et al., 2004). The Ventersdorp group then comes on top of the Central group. It comprises ultramafic and mafic lavas from the Klipriviersberg which lies below the mixed mode volcanic and sediments of the Platberg and Pniel groups. The Transvaal supergroup overlays with all its clastic and carbonate sediments. The composite Witwatersrand basin fill is now transformed into a mixed facies grade (Jolley et al., 2004; Phillips, 1987).

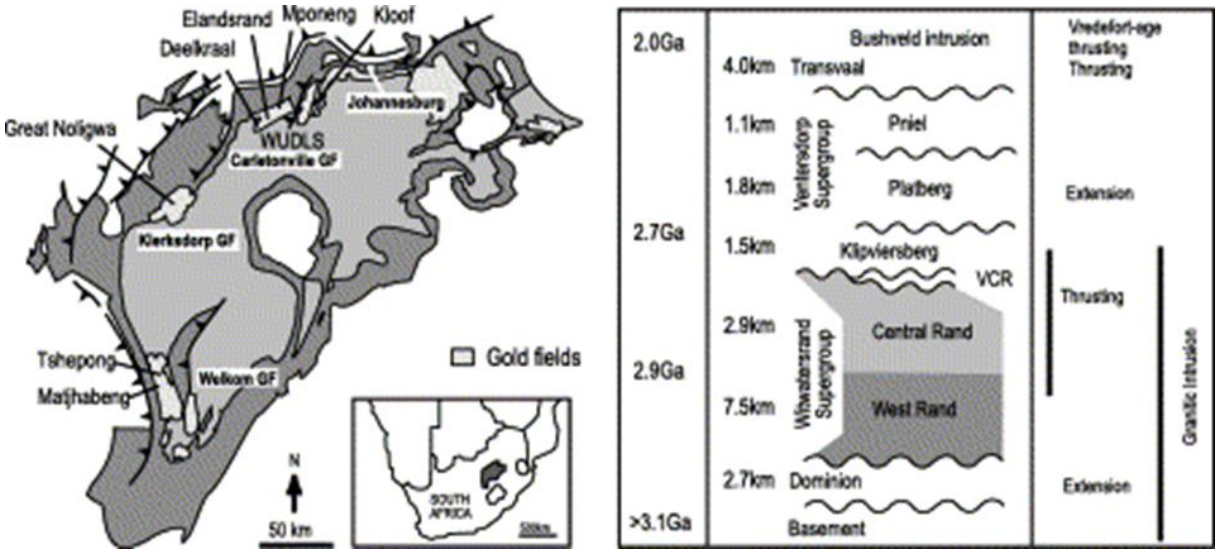

Figure 1. 1: (a) The Witwatersrand Basin covering Welkom, Klerksdorp, Carltonville and Johannesburg (left image). (b) the geological structure of the Witwatersrand super group and Ventersdorp super group (right image).

South African gold mining involves digging ore from under the surface of the earth. This ore is then processed for the extraction of gold. Uranium (^{238}U) is also brought to the surface during mining since both metals are found in the auriferous ore bodies (also called reefs) of areas around the Witwatersrand (Winde & Sandham, 2004). Thus, uranium was produced as a by-product of gold extraction from gold-bearing ore. Numerous mining companies partake in the production of gold in South Africa. Some of the biggest in the mining industry include Harmony Gold, Anglo Gold Ashanti, Sibanye Gold, and Gold Fields. A lot of waste is generated from the blasting of rock and processing of ore due to continuous mining operations (Das & Choudhury, 2013). After milling and leaching of ore, in the mining process, the remaining ore material, which is in a slurry form (solid-water mixture), is deposited onto slime dams (Winde & van der Walt, 2004). The use of sulphuric acid in the leaching process achieves about 90% extraction of ^{238}U initially present in the ore (Ford, 1993). From this, it can be expected that the uranium concentration in the tailings, which are no longer leached, will increase tenfold (Winde & van der Walt, 2004).

A tailings system is such that a mixture of water and finely ground solids (i.e., slurry) is contained in an engineered containment to reduce seepage into the environment. Water

movement into the tailings is from water in the tailing's slurry and rainfall. Seepage into groundwater is the main cause of concern for contamination (Hansen, 2015). Around 6 billion tons of tailings have been produced in the Witwatersrand since mining activities started in 1886 (Janisch, 1986). Slime dams from gold mining contain ^{238}U concentrations higher than tailings generated from conventional ^{238}U mines. The ^{238}U concentration on tailings from gold mines averages around 100 ppm and exposes approximately 600,000 t of U_3O_8 to the biosphere (F. Winde & A. de Villiers, 2002). The Witwatersrand area covers a surface space of approximately 400 km^2, and therefore an environmental pollution situation will cause problems on a large scale (Robb & Robb, 1998). Naturally occurring uranium (^{238}U) is a radioactive nuclide. Radioactivity is the process of spontaneous emission of energy in the form of particles or electromagnetic radiation by unstable nuclei (L'Annunziata, 2007). Naturally occurring ^{238}U is a strong alpha particle emitter with some beta particle emission. It has a long half-life, as a result, has a low level of radioactivity. The bone and kidneys are the primary deposition sites of ^{238}U in the body; thus, they have chemical toxicity towards the two and other organs (Brugge & Buchner, 2011). In addition, the biokinetic considerations indicate that uranium travels to and is absorbed by human organs such as the gastrointestinal tract and the liver (Bangotra et al., 2021). Secular equilibrium in the uranium decay series is when the decay rate of the daughter isotope (^{234}U) is the same as that of the parent isotope (^{238}U) (Kanai & Sakamaki, 1994). The transportation of ^{238}U in water can be determined by the $^{234}U/^{238}U$ ratio because ^{234}U is more mobile in water than ^{238}U (Veerasamy et al., 2023).

1.2 Problem statement

Gold mining has been taking place in South Africa since the late 1800s in regions including the Gauteng, North West and Free State provinces. In the gold mining process, radioactive uranium (^{238}U) is produced as a by-product. Since some of these mining activities occur near land inhabited by people and animals, there might be risk of exposure from the uranium through several pathways, such as soil and water contamination, during and after operations have ceased. Uranium contamination in the water near gold mining areas has been found in several studies (Kossoff et al., 2014; Schonfield et al., 2014). Efforts from the government to force mining companies to take responsibility for rehabilitating and minimising exposure of radioactive material to the environment and communities near previous mining sites have been

difficult. Therefore, it is important to determine the levels of contamination and identify the potential risks to people and the environment at present and in the future.

1.3 Aims and objectives

This study aimed to determine uranium concentration and its partitioning in sediment and water in different surface water bodies around mining operations in Klerksdorp, West Rand (North West province), Welkom (Free State province) and East Rand (Mpumalanga province).

The objectives were to:

- Determine ^{238}U, ^{235}U, and ^{234}U activity in sediments from river systems.
- Determine ^{238}U, ^{235}U, and ^{234}U activity in water from river systems.
- Estimate the uranium partitioning coefficient between sediment and water.
- Calculate the $^{234}U/^{238}U$ ratio in the water.

1.4 Dissertation Outline

This mini-dissertation consists of five chapters, where Chapter 1 outlines a brief introduction of the main subject and objectives of this study. Chapter 2 contains supporting literature on studies related to the topic of this study such as uranium contamination and radiation detection. Chapter 3 describes the materials and methods used in the determination of uranium activity concentration. Chapter 4 presents the results obtained and discussions. Lastly, Chapter 5 provides a summary of the conclusions of this study.

Chapter 2: Literature review

2.1 Gold mining in South Africa

The auriferous reefs in the Witwatersrand Area, which cover Gauteng, North West, Free State, and Mpumalanga, have been found to contain 100 ppm – 300 ppm of uranium levels since mining began in the late 1880s (Cole, 1998). However, these levels are lower than those of other countries such as Canada and Australia, where uranium levels range from 5000 – 50 000 ppm, and the South African ores of U_3O_8 are considered low-grade minerals (Winde & Sandham, 2004). The Witwatersrand basin accommodates numerous mining regions, as shown in Figure 2.1 (Schonfield et al., 2014). During the initial gold mining activities, uranium was dumped onto tailings dams and milling tailings without extraction or processing from the mined ore. However, during the cold war era in the 1950s, this changed as uranium was recognised as a strategic resource. In 1952, the South African government commissioned the first uranium recovery plant as part of its uranium development programme (McLean, 1994).

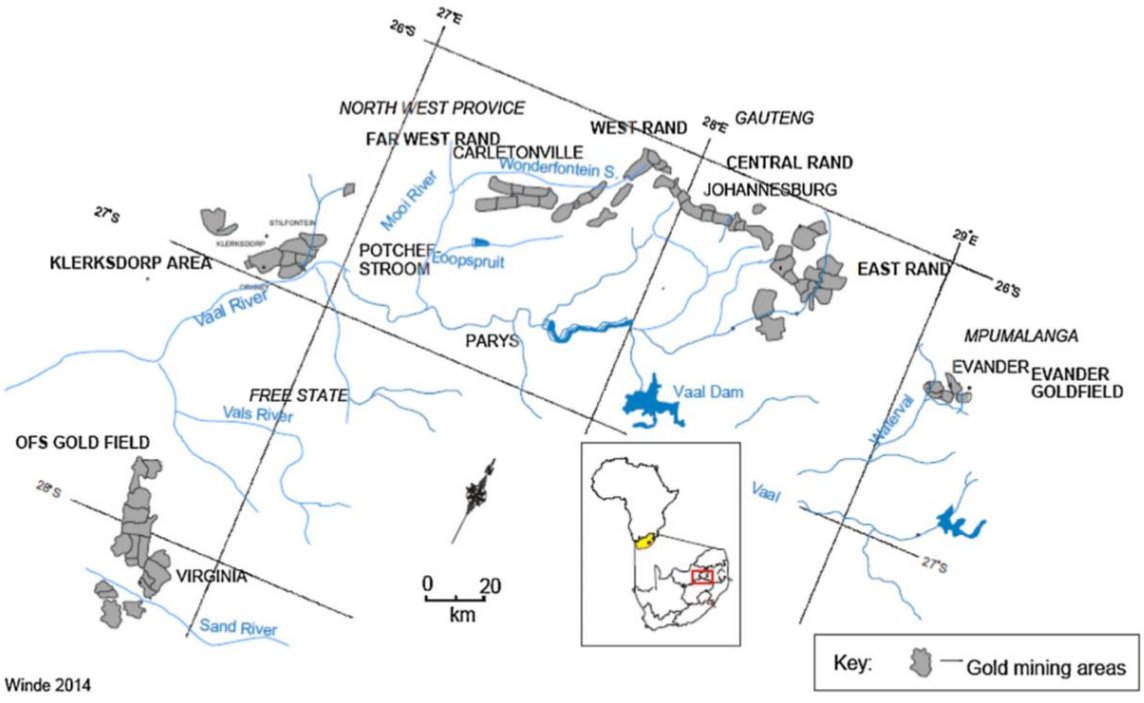

Figure 2. 1: Gold mining regions in the Witwatersrand Basin.

There are numerous methods of mining in South Africa. These include block mining, cut and fill, drift and fill, and room and pillar mining (Perold, 2013). The most common method used is the drill and blast method, where miners drill holes into the rock, fill them with explosives to blast the rock, and then use a jack-leg drill to access the gold ore. Once the ore is obtained, it is transported to the surface via a scaling bar.

The South African mining methods have unique characteristics (Perold, 2013). Moreover, the different methods can be described as follows:

- *Block and caving*: the method used for very steep ore bodies. An undercut with haulage is driven and positioned below the ore body. Holes are drilled into the ore body and blasted. The blasted ore will then fall into the undercut and hauled out.
- *Drift and fill*: the method used in reefs which are flat lying. Conventional narrow reefs are developed above the deep lying ore bodies to relieve stress on the stooping areas. Cemented mill-tailings are then filled into the stopes once the ore has been extracted.
- *Cut and fill*: this method involves cutting ore in horizontal or slightly inclined slices. Waste rock or sand is then used to fill the extracted areas.
- *Room and pillar mining*: this method is used for flat ore bodies. Pillars are placed in a pattern to support the roof. Rooms are then mined out in series. These stopes are then closed out or filled by collapsing the roof by removing the pillars, starting with the pillar furthest from the stope entrance.
- *Shrinkage and stopping*: for ore bodies with a steep dip. Blasted ore is used to support the surrounding rock on the stope. The mines then work through each section of the ore. Some amount of worked ore is removed to gain access to another section of ore rock which needs to be blasted. Once all the ore body has been broken, the stope is then emptied.

2.2 Sources of uranium pollution

2.2.1 Sources

- *Tailings dams*. The uranium contained in tailings can leak and pollute the environment through natural pressures, especially if the tailing structure loses its integrity (Dogan et

al., 2021). In South Africa, uranium accumulation in current and abandoned tailings dams around the former and current gold mining areas remains (Wolkersdorfer et al., 2021). Around 27 residues which include tailings and waste rock piles, are currently known and understood to be contributing, to some small or large extent, towards the pollution of surface waters within the whole Witwatersrand basin (Wolkersdorfer et al., 2021). When exposed to surficial processes, most of the gold mine tailings within the Witwatersrand Basin produce dust containing toxic heavy metals, semi-metals and radionuclides, which have spread across the landscape (Njinga & Tshivhase, 2017; Nwaila et al., 2021).

- *Underground ore bodies*. Uranium-bearing ore, such as uraninite, emanating from mining activities, can cause groundwater pollution because of the instability of the uraninite when it reacts with oxygen. Uranium may be stripped off ore bodies when acid mine water, which might have flooded old mining areas, gets in contact with certain rocks. This might cause a long-term source of pollution.
- *Pumped underground mine-water*. Water from underground mines moves through cracks of uranium-bearing reefs as it is pumped to the surface; the water leaches uranium from such interaction and therefore carries it to the surface where it will have the potential to pollute the surface environment.
- *Uranium accumulation in fluvial sediments*. Uranium is retained in fluvial sediment from polluted water streams, and whilst this helps to reduce pollution further downstream, the accumulation of the immobilised uranium in the sediments may become a secondary source of pollution (Winde & van der Walt, 2004).

2.2.2 Exposure pathways

There are four potential exposure pathways through which uranium can be transported to the environment, animals, and people near mine tailings (Winde et al., 2019). Figures 2.2 and 2.3 illustrate such pathways.

- *Water pathway*. Rainwater seepage and dissolved uranium pollute groundwater and streams, which are sources of life for people and animals. Drinking water from

boreholes and streams directly exposes people and animals (Winde et al., 2017; Winde et al., 2019).

- *Geophagia pathway*. This is where uranium containing material, such as soil, is intentionally or unintentionally ingested. Sediment applied to the skin with the intention of healing lesions can also lead to uranium-containing material being introduced into the body (Winde et al., 2019).
- *Food pathway*. Secondary exposure to humans can result from eating vegetables and plants irrigated with polluted water and growing on polluted soil. The ingestion of meat from animals grazed on polluted plants and drank polluted stream or borehole water also forms a secondary exposure to people as depicted in figure 2.3 (Winde et al., 2017; Winde et al., 2019).
- *Air pathway*. Heavy air blowing towards human settlements near tailing dams transport dust from the tailings material which people might then inhale. Informal settlements, which are right on top of tailings, such as the Tudor Shaft settlement, may have direct exposure to radon gas (^{222}Rn), a decay product of the uranium chain (Chambers et al., 1989; Winde et al., 2019).

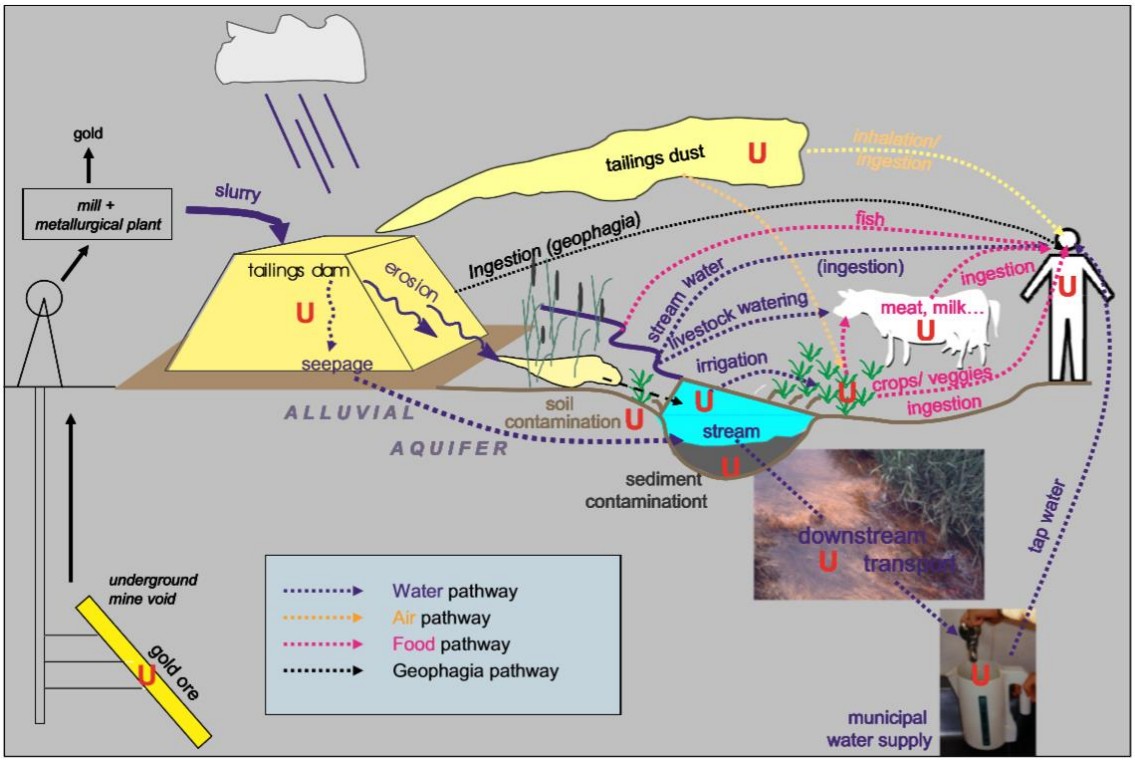

Figure 2. 2: Pathways of uranium exposure from gold tailings to humans.

Figure 2.2 illustrates the pathway of uranium from tailing dams, through the water streams to the water body that supply municipal water consumed by the public (Winde et al., 2019). The pathway includes, inhalation of tailing dust, ingestion of geophagia, irrigation and soil contamination.

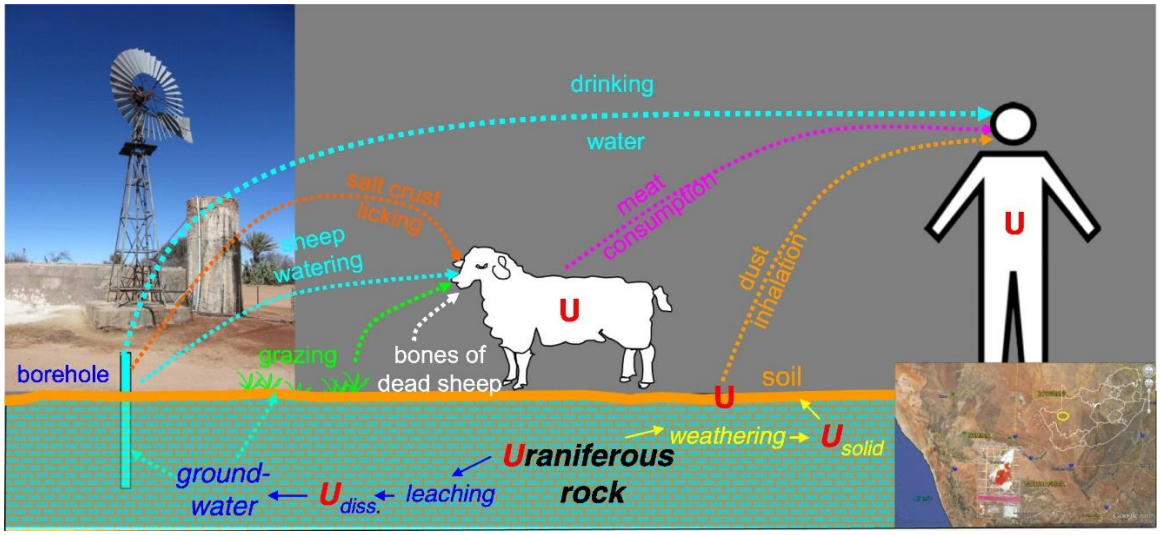

Figure 2. 3: Pathways of uranium exposure from uraniferous rock to humans.

2.3 Uranium contamination of waterbodies

Tailings seepage through underlying aquifers, and dissolved contaminants from tailings dams migrate into water streams (Winde & Sandham, 2004). The increasing depth of pore water has been shown, through piezo-metric measurements, to cause the formation of a phreatic surface inside tailings dams as seen in figure 2.4 (Funke, 1990).

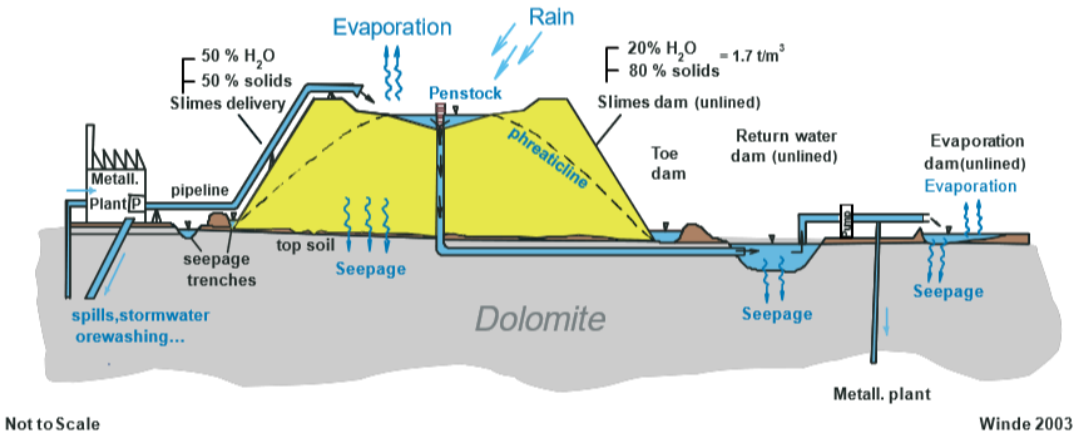

Figure 2. 4: Phreatic formation inside tailings dam.

Since tailings dams are several meters above ground, the water on top of the tailings is higher than the groundwater below the surface. This height difference produces a hydraulic gradient

that pushes the tailings water into aquifers and adjacent streams, as seen on Figure 2.5 (Winde & Sandham, 2004).

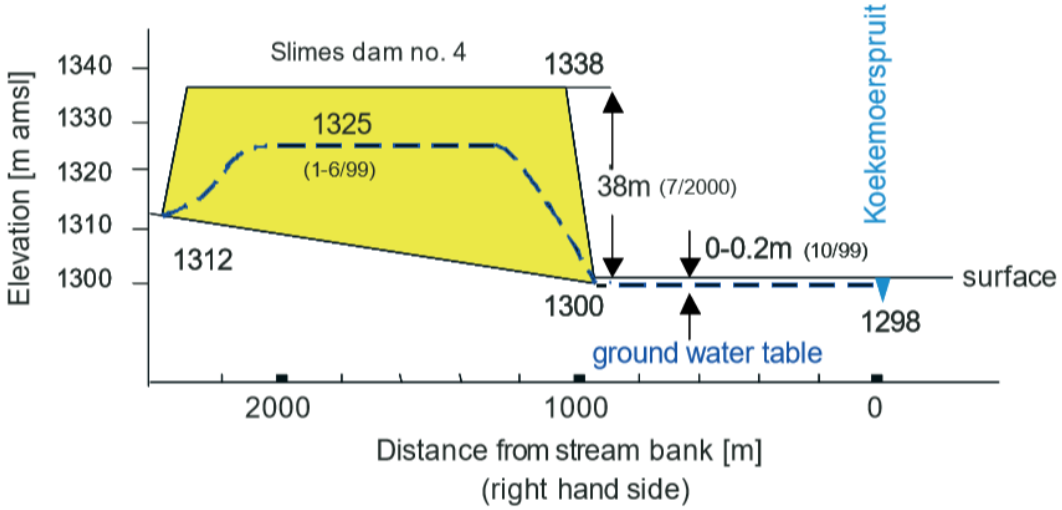

Figure 2. 5: Hydraulic gradient push of tailings water.

This water outflow from tailings is known as seepage, which may lead to contamination of underground water, streams, and sediment (Winde & Sandham, 2004), as shown in Figure 2.6 (Winde & van der Walt, 2004).

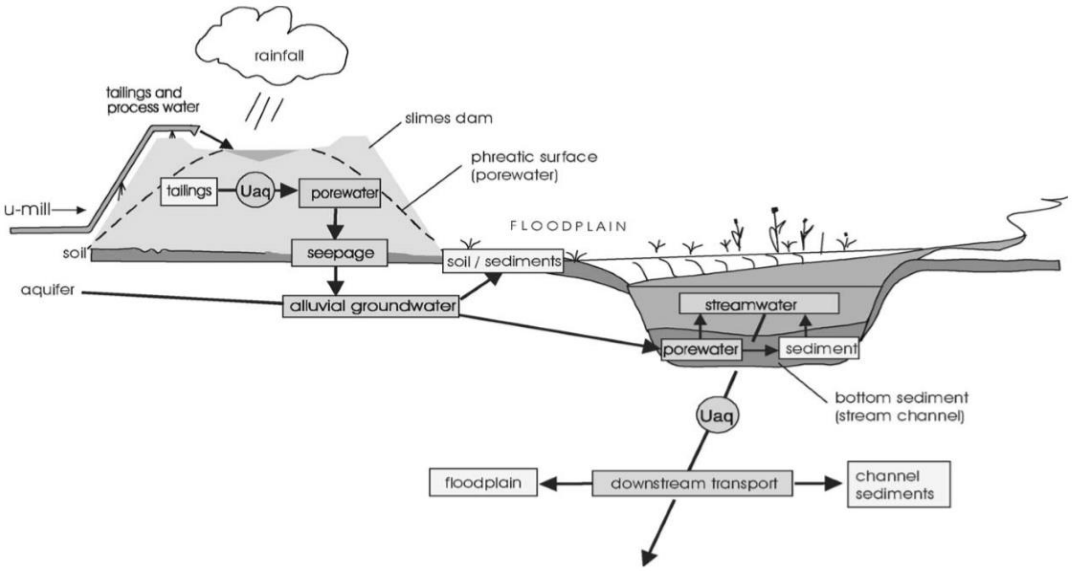

Figure 2. 6: Seepage effect on sediment and water streams.

2.3.1 Contamination of Streams

Contamination into streams via the movement of seepage from tailings is displayed in Figure 2.6. Furthermore, studies have shown that uranium levels in streams have been significantly lower than in underground water (Venter, 2001; F. Winde & A. B. de Villiers, 2002). Levels ranged from 0.05 ppm to 0.07 ppm. In some streams, uranium concentration was higher than the actual ore mined in the same area, for example, the Grootspruit stream near the Evander Goldfields and Blesbokspruit streams near East Rand Goldfields (Winde & Sandham, 2004).

2.3.2 Contamination of groundwater

Streams are connected to slime dams through alluvial aquifers in floodplain sediments. The seepage then infiltrates the streams from tailings via floodplains. Uncontaminated groundwater will then dilute seepage water, thus resulting in a lower concentration of uranium than in the incoming seepage. A mechanism of groundwater contamination is the pH precipitation of uranium from tailings' seepage into groundwater (Abiye & Shaduka, 2017). During this process, uranium interacts with alkaline dolomite material at the base of the tailings. Although underground water has been found to have uranium concentration levels (0.54 - 0.58 ppm) above limits for discharge-unweighted global mean for fresh water (0.0004 ppm), these levels were lower than the undiluted seepage of tailings under which the ground water passes. For example, alkaline underground water (pH 7.8) from floodplains in Koekemoerspruit (Winde & Sandham, 2004).

2.3.3 Contamination of sediment

Polluted water can deposit uranium in the sediment beneath it with continuing immobile uranium in the water (Winde & Sandham, 2004). Sediment sulphate crusts in the Koekemoer area were found to have uranium concentration levels (1192 ppm), which were higher than tailings dam concentration (127 ppm) in the same area. These crusts form due to the evaporation of ground water, which has risen to the surface of floodplain sediments (Winde, 2001). Contamination of sediment and waterbodies has been discussed in the section 2.3.2 and 2.3.4. Since these two mediums can be contact with each other, e.g., dams and streams with

sediment at the bottom, the distribution coefficient of uranium in water and sediment will be determined in section 4 of this paper using the following equation:

$$K_d = \frac{C_s}{C_1} \quad [1]$$

Where, K_d is the distribution coefficient, C_s is the nuclide activity concentration in sediment, and C_1 is the nuclide activity concentration in water (Payne et al., 2011).

2.4 Chemistry of uranium

2.4.1 Oxidation states and their solubility

Several factors influence the solubility of uranium. These include oxidation states, the pH and ligand type of solutions (Geipel & Bernhard, 2008). Uranium (IV) has low solubility in medium to high pH conditions. In very low pH conditions, it does not have such low solubility. In solutions containing only weak ligands, the formation of uranium (IV) colloids is probable. The most soluble and thus highest migrating state of uranium states is uranium (VI) (Lapworth et al., 2021). The formation of strong complexes from the presence of sulphates enhances solubility.

2.4.2 Reaction with sulphates

Phosphogypsum has been found to contain uranium in sulphate and phosphate complexes (Geipel & Bernhard, 2008; Lapworth et al., 2021; Papanicolaou et al., 2010). Uranium migrates easily into the environment through its reaction with sulphates. However, its migration to underground water is impeded by high pH uranium precipitates from tailings (Burnett &

Elzerman, 2001; Lysandrou & Pashalidis, 2008). This immobilisation of uranium then leads to deposition into sediment around the tailings dam.

Uranium (IV) sulphate formation. Uranium (IV) forms the strongest sulphates. Molecules of SO_4^{2-} and H_2O arrange binary sulphate complexes at low pH levels. As the pH increases it increases hydrolysis, causing competition between the OH^- and the sulphate.

This then forms two basic sulphates, which are indicated in equations 1 and 2 (Guillaumont et al., 2003; Henning et al., 2008).

$$U^{4+} + SO_4^{2-} \leftrightarrow USO_4^{2+} \quad [2]$$

$$U^{4+} + 2SO_4^{2-} \leftrightarrow U(SO_4)_2(aq) \quad [3]$$

Uranium (VI) sulphate formation. The short bonds between the uranium (VI) and oxygen elements in the uranium (UO_2^{2+}) contribute to its stability in the entire pH range (Henning et al., 2008). When a water molecule has high acidity protons, it causes the transformation of an adjacent free water molecule into a Bronsted base which helps form this uranium complex.

Sulphate complexes are formed by the uranium ion under acidic solutions, whilst ternary complexes are formed under solutions of pH >3. And these complexes include;

$(UO_2)_2(OH)_2(SO_4)_2^{2-}$,$(UO_2)_3(OH)_4(SO_4)_3^{4-}$, and $(UO_2)_5(OH)_8(SO_4)_n^{2-2n}$ where $n = 5{,}6$

(Moll et al., 2000).

Different pH environments can host three sulphates species of uranium (VI) (Guillaumont et al., 2003):

$UO_2^{2+} + SO_4^{2-} \leftrightarrow UO_2SO_4(aq)$ $\quad logK^0 = 3.15 \pm 0.12$

$UO_2^{2+} + 2SO_4^{2-} \leftrightarrow UO_2(SO_4)_2^{2-}$ $\quad logK^0 = 4.14 \pm 0.07$

$UO_2^{2+} + 3SO_4^{2-} \leftrightarrow UO_2(SO_4)_3^{4-}$ $\quad logK^0 = 3.02 \pm 0.38$

2.4.3 Speciation under different conditions

The oxidation states of uranium (+3,+4,+5, and +6) have a great influence on its behaviour, and the most common uranium oxidation states in nature are U(IV) and U(VI) (El-Sharkawy, 2018). Depending on the environment it finds itself in, Uranium can bind to different complexes. In most natural waters, uranium has been found to exist in the form of the less hazardous tri-carbonate species (Geipel & Bernhard, 2008) compared to phosphates and citrate species. The speciation of uranium in contaminated water can be affected by weather conditions. In winter seasons, uranium (VI) is more dominant, while uranium (IV) finds itself more dominant during the summer seasons (Phrommavanh et al., 2008). Many factors, including the availability of uranium or its parents in the aquifer matrix and the geochemical and hydro chemical conditions present, affect the activity concentration of uranium in natural waters (Duff et al., 2002). The temperature may influence the stability of uranium, especially the more mobile uranium (VI) species. A decrease in temperature decreases the stability constant of the uranium (VI) complex (Vetesnik et al., 2008).

2.5 NORMs

Naturally occurring radioactive materials (NORMs) exist in the environment at low background activities (Koppel et al., 2022). They naturally rotate and partition in the environment, reflecting the different processes and chemistries in those environments (Cresswell et al., 2020).

2.5.1 Radioactive equilibrium

Radioactive equilibrium occurs when the activity of the parent nuclide is similar to that of its intermediate or final daughter product. This also implies that the rate of radionuclide decay in a particular isotopic series is the same (Papadopoulos et al., 2013). This secular equilibrium can be disturbed by various activities, and when this happens, the parent radionuclide or the daughter product can be removed. Radionuclides can be mobilised through activities involving geochemical processes where the soluble radionuclides of a certain decay series are dissolved and precipitated (Gascoyne, 1992). A system has attained steady state when there is no longer a change in the rates at which each nuclide decays, which is another way of saying it is in a state of secular equilibrium. Examples include the interactions between the long-lived uranium and thorium isotopes, Uranium-238 (^{238}U), Uranium-234 (^{234}U) and Thorium-232 (^{232}Th).

2.6 Biological effects of radiation

Radioactive isotopes mainly comprise of the species present in the decay chain series of Uranium-238 (^{238}U), Thorium-232 (^{232}Th), and Potassium-40 (^{40}K) (Salazar et al., 2021). Radionuclide accumulation and increases in radioactivity above critical levels may lead to health risk and environmental damage (Ali et al., 2018; Garner et al., 2015; Xhixha et al., 2015). ^{238}U has a half-life of 4.5 billion years and ^{232}Th has a half-life of 14.05 billion years as indicated in figures 2.7 and 2.8 respectively. The figures further display the decay series of ^{238}U and ^{232}Th with the half-lives of the decay daughters involved and the particle emissions from one daughter to the other. Radiation can cause acute or chronic damage to the liver. DNA damage and oxidative stress are amongst the early effects of radiation. The production of reactive oxygen species causes cell apoptosis in the liver and acute inflammation.

The early acute liver radiation damages can be repaired since the liver is a delayed response organ, but if appropriate clinical treatment is not administered it might lead to radiation-induced liver damage (RILD) (Li et al., 2021). ^{238}U is an alpha particle emitter and it also emits weak gamma particles. Alpha particles have a weak penetrability compared to other particles and they pose minimal hazard as long as they are outside of the body. However, alpha particles can be dangerous to organs and tissues, leading to kidney failure and paralysis if inhaled or ingested into the body (Van Eeden et al., 2009).

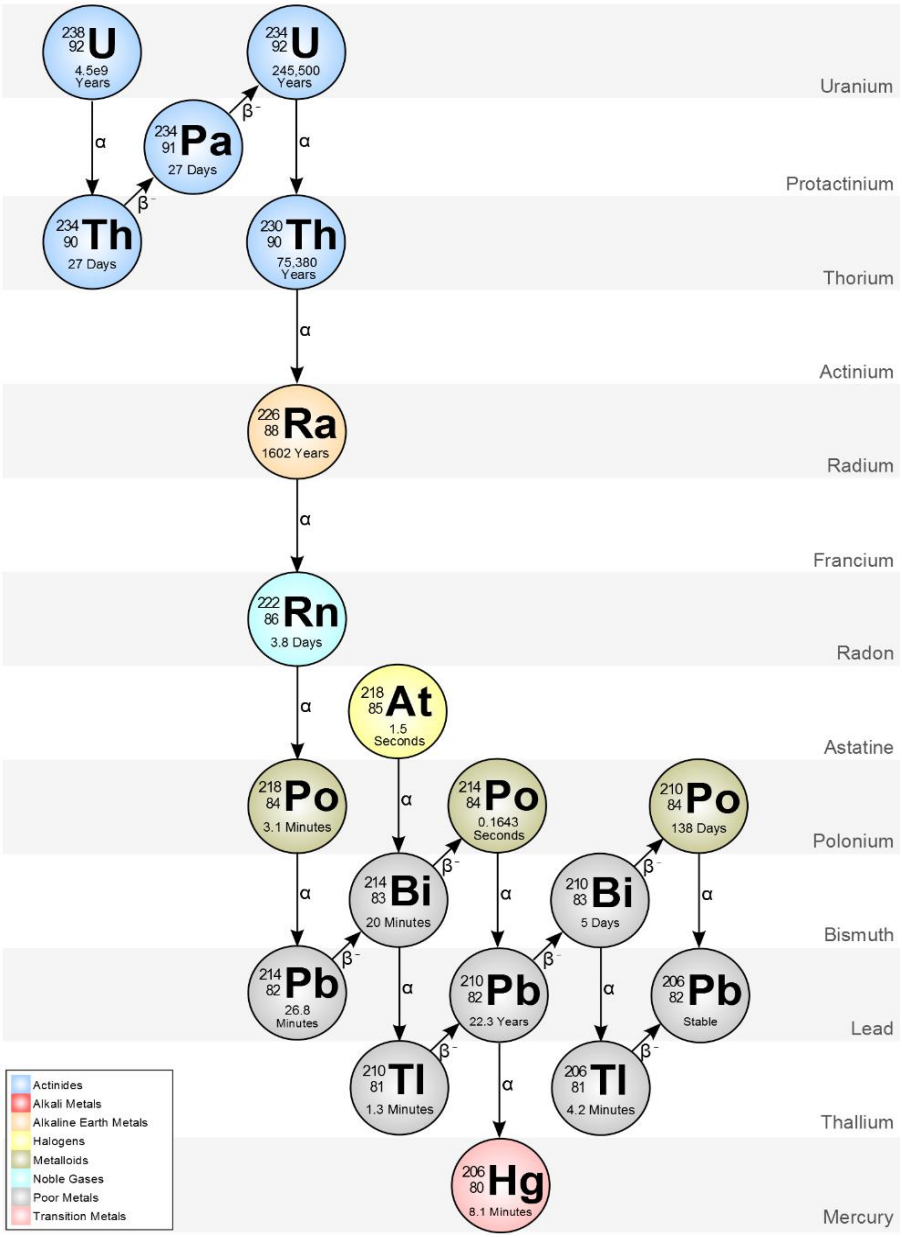

Figure 2. 7: Uranium decay series.

Uranium decay (as seen in Figure 2.7) starts with 238U, the long-lived parent. After 14 decay stages involving its daughter products which have different half-lives of seconds, minutes, days, years, and thousands of years, the series ends with lead (^{206}Pb), which is a stable isotope (Choppin et al., 2013). The daughters emit gamma rays in many of these steps at energies which are specific to the decaying radioisotope. Some daughters in the decay chain, e.g., ^{214}Pb and ^{214}Bi, can be used to determine the ^{238}U content since it does not have gamma rays which can be used for detection. The radioactive equilibrium which usually occurs between the parent

and daughter products, the concentration of the parent can be determined through the measurement of the gamma radiation from the daughters (Killeen et al., 2015). The concentration of ^{232}Th in the earth's crust is about 6 ppm (3 times more than that of ^{238}U), making it the most abundant naturally occurring radioactive element. Monazite, which is a rare earth mineral, is where ^{232}Th is commonly found in the composition $(Ce, La, Nd, Th)PO_4$ (Yu et al., 2022). Mining and processing rare earth metals consequently lead to thorium contamination in the environment (Li et al., 2019; Maes et al., 2017; Su et al., 2021; Wang et al., 2018). There has been great concern over the health risks thorium poses to humans and the environment (Ali et al., 2019; Shukla et al., 2020). When thorium enters the blood circulation after inhalation, ingestion, or infection through a skin wound, about 75% deposits into the liver and bones, with some small fractions going to kidneys and soft tissue (Creff et al., 2019).

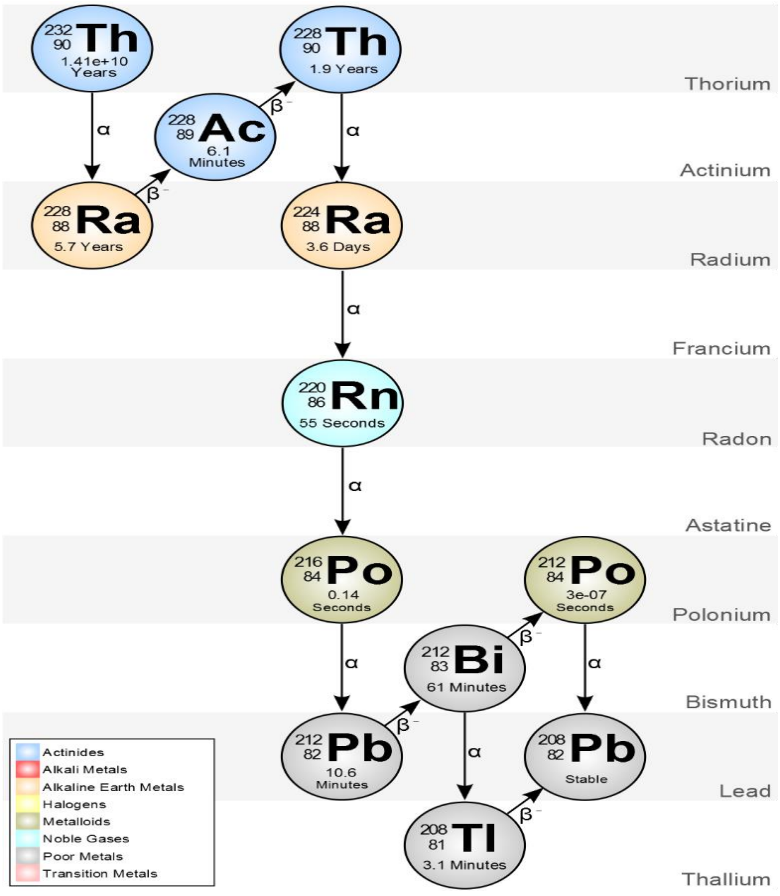

Figure 2. 8: Thorium decay series.

The thorium decay chain (figure 2.8) also starts with the long-lived parent, ^{232}Th, and after 10 decay stages the series ends with another lead (^{208}Pb) stable isotope (Choppin et al., 2013). As

in the case of ^{238}U series, gamma rays are emitted in many of the stages at energies specific to the decaying radioisotope. ^{232}Th does not emit gamma rays and thus its content can be determined indirectly through the detection of gamma rays from its daughter Thallium (^{208}Tl). The ^{232}Th chain, unlike that of ^{238}U does not have many daughters with extremely long half-lives. The daughter with longest half-life in the ^{232}Th series is Radium (^{228}Ra) with 5.7 years (Killeen et al., 2015). The hazards of uranium and thorium to the environment, human and animal life have been discussed and it is observed that continual exposure to such radionuclide may lead to detrimental circumstances. A study of the levels of exposure from uranium and its progeny in the Witwatersrand basin which covers 3 provinces in South Africa is reviewed next.

2.7 Radiation detection

2.7.1 Gamma spectroscopy

Gamma-ray spectrometry is a technique used to identify radioactive isotopes in a sample, in a non-destructive manner. The energy of the incident gamma ray is measured by the detector. The identity if the incident gamma ray can be discovered by matching it with the energy of a known radioisotope (Pavan et al., 2019). The measurement of samples with gamma spectrometry involves, firstly, the storing of the sample material in sealed containers using sealant like beeswax to ensure that secular equilibrium is reach between radon and its progenies (Vukanac et al., 2022). After a couple of weeks, the samples are then measured with the germanium semiconductor HPGe detector. The Genie 2000 software from Canberra can be used to record all spectra, and Genie 2000, Aptec, and Anges software can be used to analyse the spectra. The range of measurement periods can vary and reach 250000 seconds (Valković, 2019). Direct measurements of the specific activity such as ^{235}U can be made using its energy peak on the spectra or its whole energy peak corrected for radium-226 (^{226}Ra). Thorium-234 (^{234}Th) at 63 keV peak energy or Protactium-234 (^{234m}Pa) at 1001 keV can be used to determine ^{238}U. Background noise, dead time, and coincidence summing effects can also be adjusted for the Net count rates The calculation of activity concentration and uncertainty includes statistical

uncertainty of up to 30% and a 5% uncertainty for efficiency calibration, whilst the measured mass uncertainty can be ignored (Valković, 2019).

2.7.2 High purity germanium (HPGe) detectors

Gamma-ray spectrometry with HPGe crystals has excellent energy resolution and allows for numerous procedures to be performed such as determination of radionuclide composition in soil; activity measurement of samples which emit gamma rays; analysis of low-level environmental samples; and preparation of standard samples (Prozorova et al., 2021). Germanium detectors are semiconductors, which have a P-type, then an intrinsic layer, and N-type contact abbreviated p-i-n. The intrinsic/depleted region commonly has a high sensitivity to Gamma and X-rays. Under reverse bias, an electric field will be established in the intrinsic region. When photons interact with matter in the depleted region of a detector, charge carriers are produced. An electric field then moves the carriers (which are holes and electrons) to the p and n electrodes. The charge then enables an intrinsic charge-sensitive preamplifier to produce a voltage pulse. The outer surface of the crystal is where the rectifying contact of a detector semiconductor junction is commonly placed. A coaxial detector is shown in Figure 2.9. The

p+ is the outer contact, and the n+ is the inner contact. The depletion layer grows inwards as the voltage increases (Mirion, 2019).

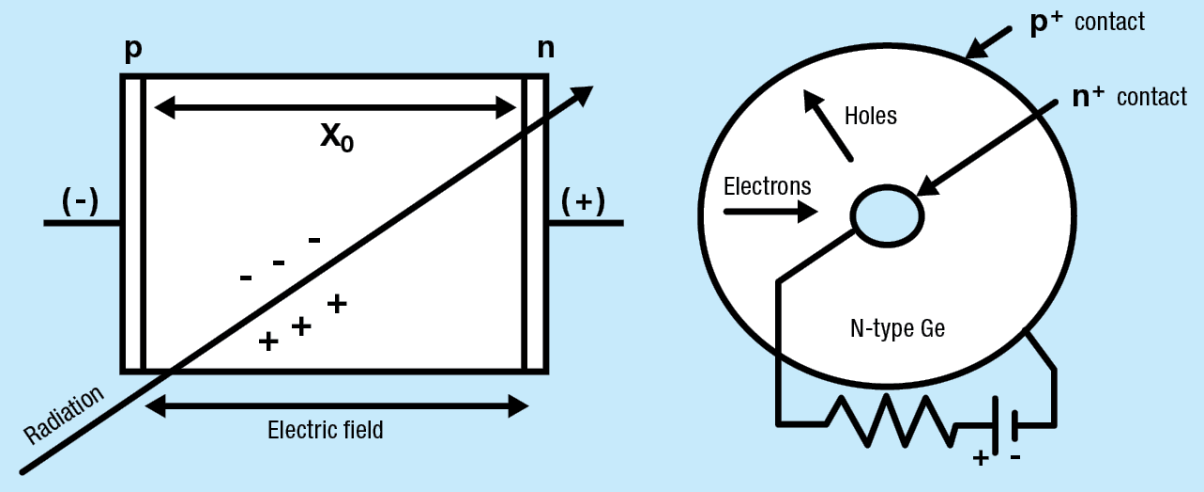

Figure 2. 9: (Left) p-i-n junction detector with reverse bias (Right) A cross-section of an n-type coaxial detector perpendicular to the cylindrical axis.

In order to control the production of charge carriers, thus preventing leakage current, germanium detectors need to be cooled because they have low band gaps. Liquid nitrogen is commonly used to cool the detectors at 77K (-195.15°C). If charge production is not controlled, then current leakage will occur and induce noise which will destroy the energy resolution of the detector (Mirion, 2019).

2.7.3 Characteristics of the HPGe detector

- The HPGe detector provides accurate and reliable information to identify radionuclides from their mono-energy gamma rays (Lohrabian et al., 2021; Olivares et al., 2017).
- The HPGe detector has an energy resolution 20 to 30 times that of a sodium iodide NaI(Tl) detector.
- A limitation of the HPGe detector is the loss of sensitivity when exposed to high-flux radiation.
- The HPGe detector offers high radiation detection efficiency when radiation sources are point sources. This helps avoid early saturation of the detector (Lohrabian et al., 2021).

2.7.4 Alpha spectrometry

Alpha-particle spectrometry is a radiometric analytical technique used to identify radionuclides and their activity in a liquid or solid form sample. This radio-analytical technique analyses radionuclides with high sensitivity and efficiency. This technique allows the use of an alpha emitting isotope of the element of interest as a tracer, thus making it a reliable method of analysis (Guirguis et al., 2015; Vukanac et al., 2022). Radionuclides must be dissolved and chemically separated from the bulk sample before a tracer source can be prepared. This is because alpha particles have a short range of travel through matter (Vadja, 2012). Tracer sources are commonly prepared for each radionuclide of interest. There are three functions that the chemical separation serves in the preparation of tracers. Firstly, it increases the yield of the element/radionuclide of interest by removing unwanted elements. Secondly, to produce a clean product by reducing unwanted elements that might affect the quality of the spectra. Thirdly, to remove all other radionuclides, which are alpha emitters and whose energy peaks might interfere with the energy peaks of the radionuclides of interest (Aggarwal, 2016). The alpha spectrometer (Alpha Analyst, Canberra, USA) can perform alpha-particle spectrometry measurements. The spectrometer has 10 passivated implanted planar silicon (PIPS) semiconductor detectors which have an active area of 450 mm^2 and 28% geometrical efficiency (for a 25 mm source disk diameter) (Vukanac et al., 2022). Standard radionuclide sources, which include radionuclides like ^{238}U, ^{235}U, Plutonium-239 (^{239}Pu), and Americium-241 (^{241}Am), may be used for the detector's energy and efficiency calibration (Vajda et al., 2020).

Genie 2000 from Canberra can be used to record and examine alpha spectra. The measurement periods can range from one to seven days, depending on the radionuclide activity in the radiochemical recovery can be measured by its activity concentration (Jia et al., 2002).

The alpha spectrum analysis report, which is generated by the Genie 2000 software, contains the uncertainty for the detected alpha activity. The statistical uncertainty, chemical recovery factor, and efficiency uncertainties are all considered in the uncertainty budget (Vukanac et al., 2022). Standard radiochemical analysis methods comprising of three steps can be used to determine the activity of ^{238}U, ^{235}U, and ^{226}Ra. These steps are: sample preparation, radionuclide separation, and source preparation (Jia et al., 2002; Vukanac et al., 2022). The preparation of the sample can be done using acid leaching by nitric acid (HNO_3), hydrofluoric acid (HF) and perchloric acid ($HClO_4$) on a hot plate (Jurečič et al., 2014; Selvig et al., 2005). Before sample digestion, the precise activity concentrations of the relevant tracers (i.e., ^{232}U for uranium determination) are added to calculate the radiochemical yield of the analysis (Vukanac et al., 2022). The separation for uranium radionuclides can be done through extraction chromatography resins, one such technique is the Uranium and Tetra Valents Actinides (UTEVA) technique which involves firstly, sample preparation in a known concentration of HNO_3. Secondly the loading of sample on the UTEVA column preconditioned with a known concentration of HNO_3, then effluent is discarded between step 2 and step 3. Thirdly, the washing of the column with known concentration of HNO_3 and hydrochloric acid (HCl), effluent is once more discarded between step 3 and 4. Fourthly, is the elution of uranium with a known concentration of HCl. Lastly, the uranium concentration is estimated using alpha spectrometry (Dalencourt et al., 2020; Prabhu et al., 2016).

The alpha source preparation for uranium radionuclides can be done in one of two ways, the electrodeposition method or the micro-coprecipitation method. The electrodeposition method involves using stainless steel disk of 19 mm in diameter from a known concentration of ammonium oxalate $(NH_4)_2C_2O_4$ and HCl electrolyte mixture (Puphal & Olsen, 1972). The applied current and deposition time may vary e.g., applied current of 0.6 A with a deposition time of 2 hours (Puphal & Olsen, 1972). The second method, micro-coprecipitation, involves Neodyum (Nd^{3+}) fluoride. Using a Gelman filter device, the neodymium fluoride suspension can be filtered through polypropylene filter paper of 25 mm in diameter and 0.1 m pore size.

The dry filter is then fixed on a stainless-steel disk (Hindman, 1983; Sill & Williams, 1981; Vukanac et al., 2022).

2.7.5 Tracers in alpha spectroscopy

Tracers have numerous functions in alpha spectrometry. They are used to determine the concentration of radionuclides and to monitor the chemical yield during separation and purification procedures (Aggarwal, 2016). There are some requirements to selecting a suitable tracer of a radionuclide of interest. These include the need for the tracer to have the same chemical behaviour as the radionuclide of focus, the tracer must have a long half-life to prevent repeated calibration from progenies, the energy of the emitted alpha particle from the tracer has to be lower than that of the radionuclide of focus in order to avoid interference with the energy peak of the desired radioisotope.

Uranium-232 (^{232}U) is commonly used as a tracer for uranium isotopes ^{238}U, ^{235}U, and ^{234}U (Aggarwal, 2016; Guirguis et al., 2015). There are other tracers used according to their suitability for specific elements. Table 2.1 indicates such tracers (Aggarwal, 2016).

Table 2. 1: Tracers commonly used for specific elements.

Element	Tracer (spike)	Remarks
Po	^{209}Po	-
Ra	^{225}Ra (β)	Measured via its daughter product ^{217}At
Th	^{229}Th	Progeny of ^{233}U
U	^{232}U	Thermal neutron irradiation of ^{231}Pa
Np	-	No useful alpha emitting tracer
Pu	^{236}Pu	Decays by α-particles or energy "higher" than all the commonly determined Pu isotopes
	^{238}Pu	Can be used, but needs one extra analysis without a tracer if ^{238}Pu in the sample is also to be determined
	^{242}Pu	Gives α-particles of energy "lower" than all the commonly determined Pu isotopes
Am	^{243}Am	High flux isotope irradiation (HFIR) of ^{242}Pu
Cm	^{248}Cm, ^{243}Cm	^{248}Cm is a daughter product of ^{252}Cf

2.7.6 Advantages of alpha spectrometry

The advantages of alpha spectrometry include the determination of alpha emitting radionuclides and beta emitting radionuclides with alpha emitting daughters. Radionuclides, which are alpha emitters with half-lives longer than the sample preparation and analysis time, can be determined as well (Vadja, 2012). The main advantage of this method is the use of pure solution of actinide to eliminate trace elements which might cause the reduction of deposition yield and the quality of the resultant alpha-spectrum (Guirguis et al., 2015). High sensitivity and low detection limits. Small sample sizes can be analysed because of the high sensitivity of alpha spectrometry. Sample sizes ranging from 1-10 g of soil can be analysed in the analysis of thorium and uranium, with detection limits from mBq to µBq per unit volume or mass (Vadja, 2012; Vukanac et al., 2022). There are some factors that enable low detection limits.

The first factor is the high yield during alpha decay. An intensity of 100% decay is indicated through the small peaks within a small energy range that alpha emitting radionuclides give. The second factor is the low intrinsic background of semiconductors which is around 10^{-5} to 10^{-6} counts per second. Third is the efficiency of the detector, which is 100% of the incident alpha particles. And lastly, the low sensitivity of the semiconductor to beta and gamma radiation. Alpha spectrometry is a reliable technique due to the use of alpha emitting tracers in its process (Vukanac et al., 2022). However, only if no radiotracer losses (through alpha particles emissions being attenuated by matter) occur before the tracer isotopes and sample are in equilibrium. The internal tracer makes up for both the counting accuracy of the detecting device and losses that occur during chemical separations. This is because the ratio of sample to tracer peak regions directly determines the outcome. As a result, precise estimations of the target radionuclides can be made without having a highly accurate understanding of the counting efficiency (Vadja, 2012). Alpha spectrometry has advantages over gamma spectrometry because of its lower detection limits, but the method is far more demanding and complicated (Vukanac et al., 2022). For instance, the long hours required for the chemical separation process to remove unwanted elements become a disadvantage of this method.

Chapter 3: Materials and Methods

The materials and methods for analysis will be outlined in this chapter. Firstly, a description of the Witwatersrand Basin, which is the study area, and its geological characteristics will be given. Secondly, the locations where samples were collected will be outlined together with the equipment utilized in collecting and packaging the samples. The instrumentation used for data analysis, including the sample analysis steps, will then be described. The various calibration activities for the instruments will also be described after that. Lastly, determining uranium isotopes in water and sediment will be done.

3.1 Study area: Witwatersrand Basin

The Witwatersrand Basin is a stretch of geological land located in the central Kaapvaal Craton and is one of the greatest gold deposits in the world (Pham, 2021). It contains gold and uranium bearing reefs (figure 3.1) deposited between 2,714 Meso-Archaean (Ma) and 2,985 Ma (Guy et al., 2012). The basin stretches over an arc of approximately 400 km, cutting across the North West, Free State, and Gauteng provinces (Riemer & Durrheim, 2012). Fracture fluids, with variable geochemical signatures and different microbial ecosystems, about 3.9 kilometres deep below the surface, have arisen due to the rock layers' mining (Lau et al., 2016; Magnabosco et al., 2018; Onstott et al., 2006). The “Witwatersrand supergroup” hosts about 7000 m of sedimentation made up of coarse- grained conglomerates in which gold is found, together with uranium, carbon seams, quartz, pyrite, and phyllosilicates (Riemer & Durrheim, 2012).
Following the discovery of these gold-bearing conglomerates in 1886, increased exploration led to the further discovery of this gold in and around the basin on the East Rand in 1914, the West Rand and Klerksdorp in 1937, the Orange Free State in 1946, as well as the Kinross area in 1955 (Durrheim, 2010).

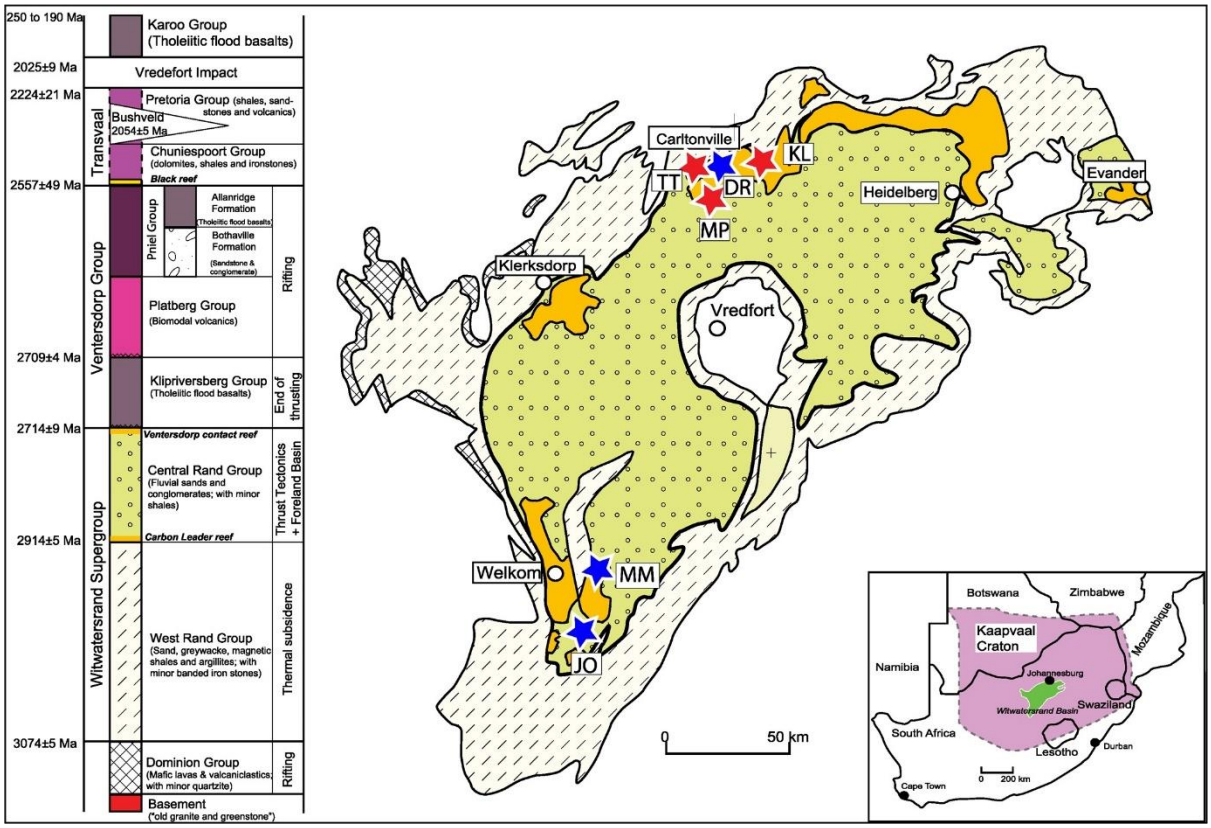

Figure 3. 1: Geological map of the study area.

The golden areas in figure 3.1 represent the five major gold fields (Welkom, Klerksdorp, Carltonville, Heidelberg, Evander). The water and sediment samples collected in this study were collected from all five regions. The abbreviated mining operations are translated as follows: JO = Joel; MM = Masimong; MP = Mponeng; TT = Tau Tona; DR = Driefontein; KL = Kloof (Li et al., 2022).

3.1.1 Geological setting

The Witwatersrand basin is an erosional and structural remnant a granite-greenstone terrane in the central part of the Archean Kaapvaal craton in South Africa. The Witwatersrand supergroup, a 7.5 km thick sedimentary succession made up of conglomerates, sandstones, quartzite, and some volcanic rock, fills the basin (Fuchs et al., 2021). The Witwatersrand supergroup rests on the uraniferous siliciclastic and volcanic rock of the dominion group, roughly 3074 Ma years old (Armstrong et al., 1991; Li et al., 2022). The Supergroup is divided into the West Rand Group (2985 Ma – 2914 Ma) and the upper Central Rand Group (2902 Ma

– 2840 Ma) (Kositcin & Krapež, 2004; Li et al., 2022). The West Rand Group is dominated by alternating sequences of sandstone and shale that accumulated during repeated cycles of marine transgression and regression. The Central Rand Group, in contrast, consists of fluvial conglomerates and sandstone deposited onto alluvial plains and separated by erosional unconformities (Catuneanu, 2001; Els, 1998). The Ventersdorp Super Group (2709 Ma), the volcano-sedimentary rocks, overlays the Witwatersrand Super Group with consistency, while the same Ventersdorp Super Group is inconsistently overlain by the Transvaal Super Group (Fuchs et al., 2021).

Gold-bearing conglomerate reefs have yielded an average gold grade of approximately 8.4 g/t from the goldfield regions stretched over 400 km from the north-eastern to the south-western margin of the basin (Frimmel et al., 2005; Tucker et al., 2016). The gold rich reefs (20 g/t to 40 g/t of gold), such as the Carbon Leader reef, which has noticeable amounts of organic matter, are found in the lower part of the Central Rand Group (Frimmel, 2018). The reefs of the middle Central Rand Group, such as the Basal and Steyn reefs, come second with gold grades of 5 g/t to 12 g/t. Following these reefs are the upper Central Rand Group and the Ventersdorp Group. The Black Reef Formation, which is just above the Pniel Group, has localised gold enriched areas (bearing < 10 g/t gold grades) which are very close to an underlying gold-bearing reef such as the East Rand goldfield (Frimmel, 2018; Fuchs et al., 2016).

3.2 Sampling procedure

Data collection methodology and procedure were applied. The basic methodological steps taken were:

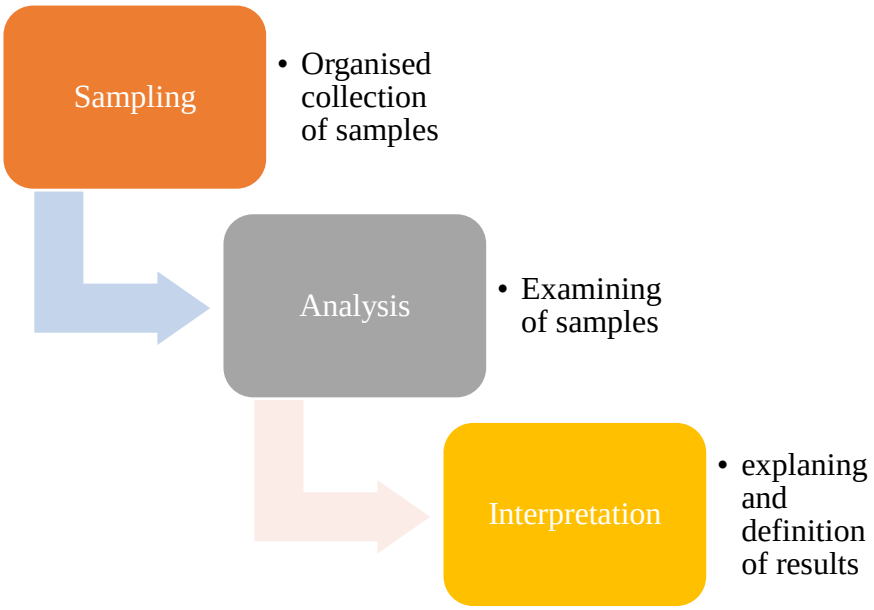

Figure 3. 2: Methodological steps for sample analysis

The specific areas and points for sampling were identified according to their proximity to mining operations and tailings dams. Their accessibility was also evaluated to consider them as realistic points of sampling. The radiological relevance of the identified points was assessed. This was done by considering the sampling plans and locations selected by the National Nuclear Regulator. The locations are sampled as part of the regulator's environmental sampling activities, confirming that reports from areas sampled upon by all mines under the regulation are true. Samples were collected along the Witwatersrand Basin in Gauteng province (West Rand), Free State province (Welkom), Mpumalanga province (East Rand), and North West province (Klerksdorp). Figures 3.3 to 3.6 indicate, some of the points from which samples were taken in each province, and Tables 3.1 to 3.4 summarise the origin and description of all samples under investigation.

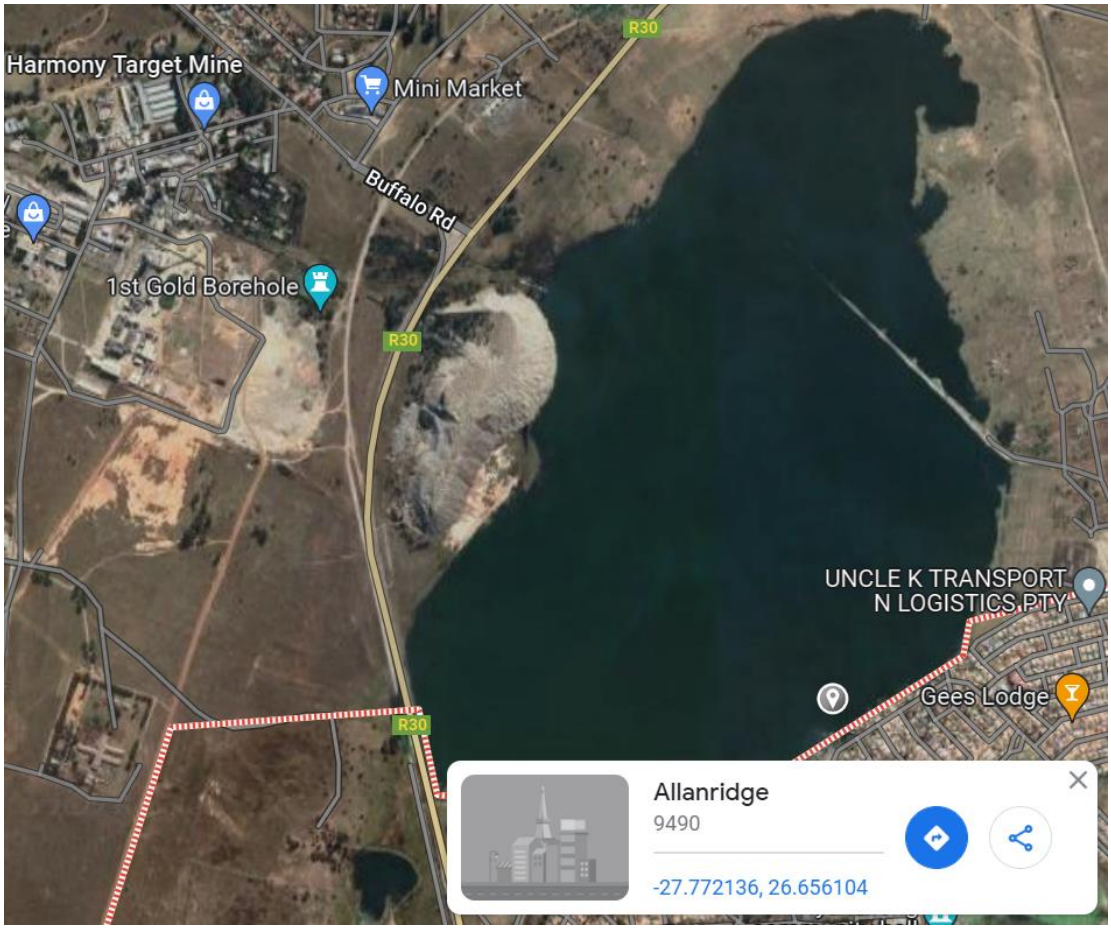

Figure 3. 3: Voelpan dam in Nyakallong township near Harmony Target Mine, Welkom (Free State province).

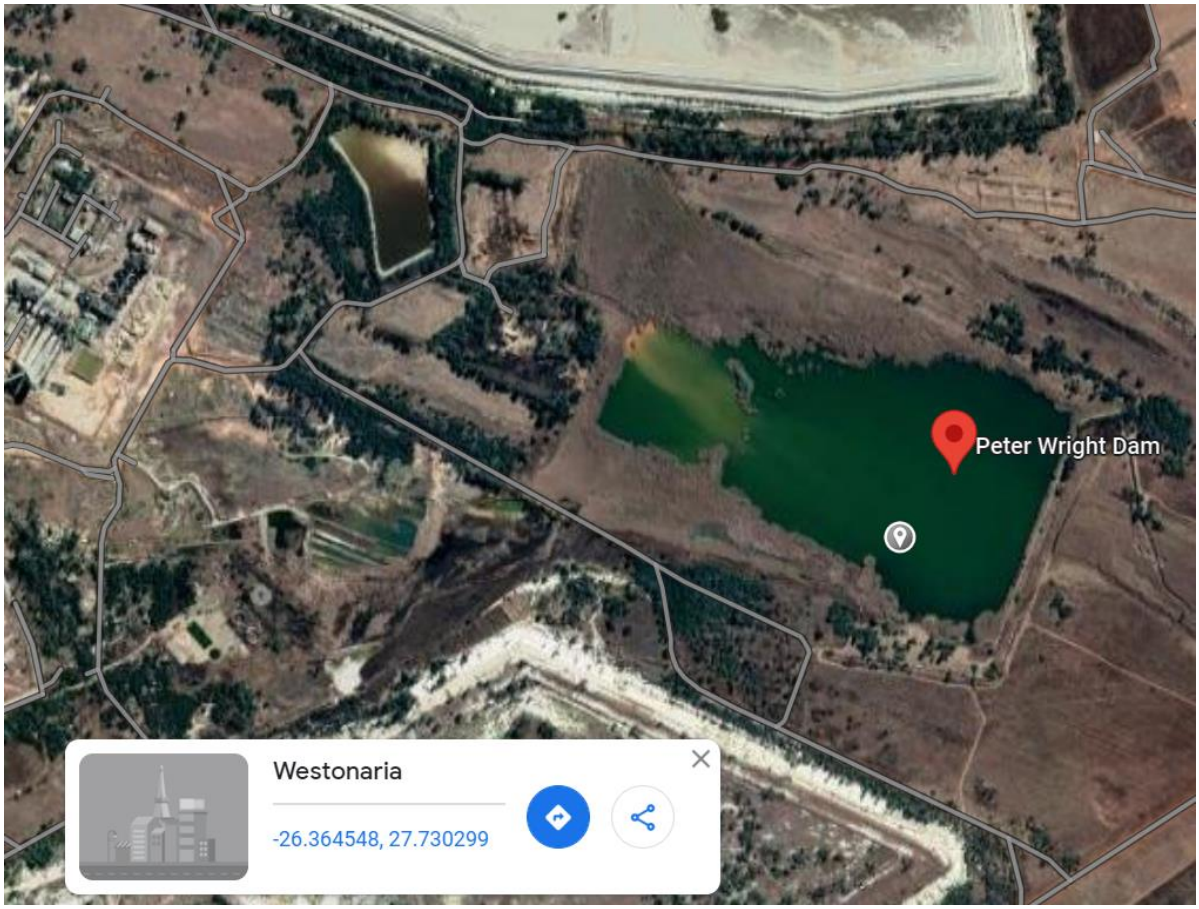

Figure 3. 4: Peter wright dam next to Ezulwini Plant, West Rand (Gauteng province).

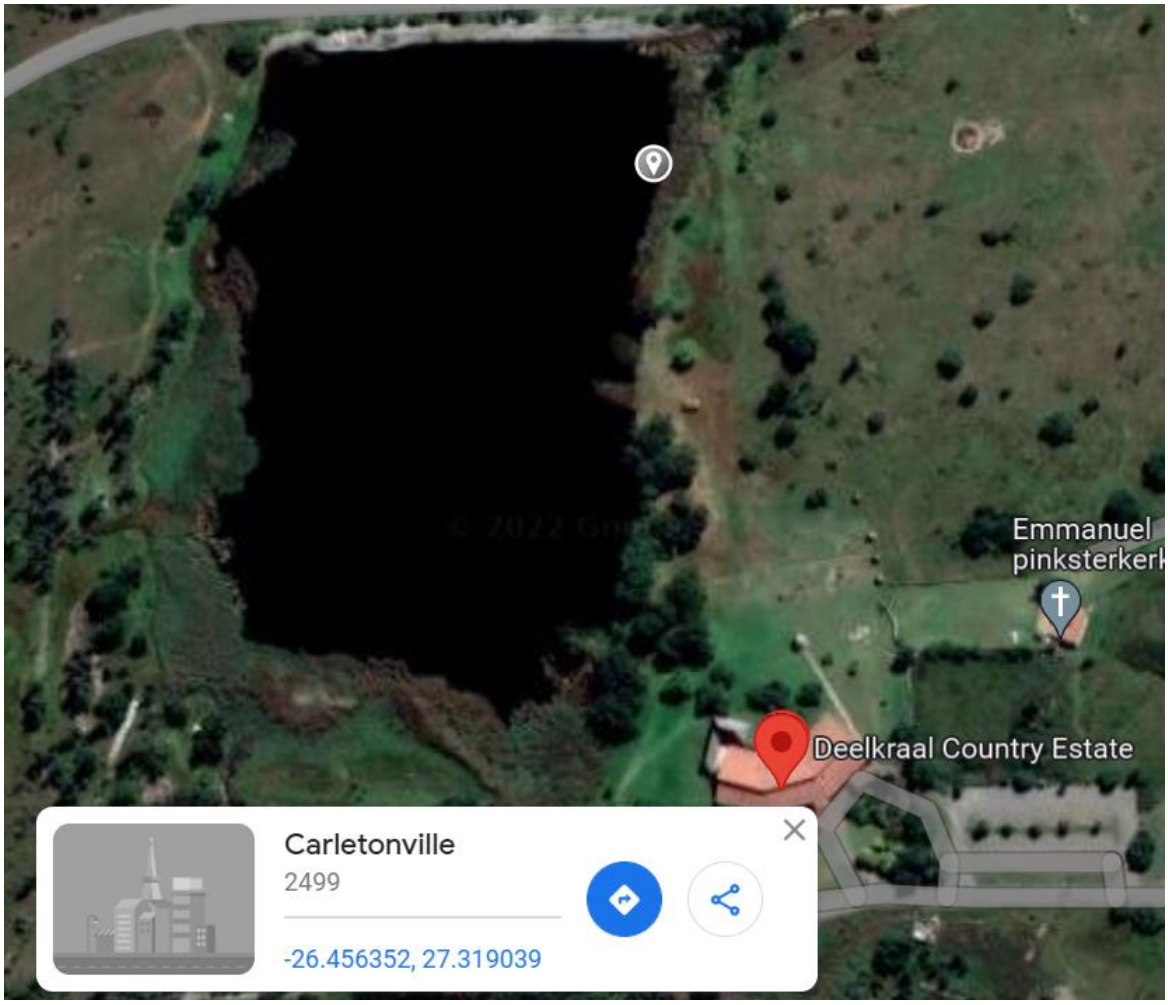

Figure 3. 5: Deelkraal dam downstream of Kusasalethu mining operations, Klerksdorp (North West province).

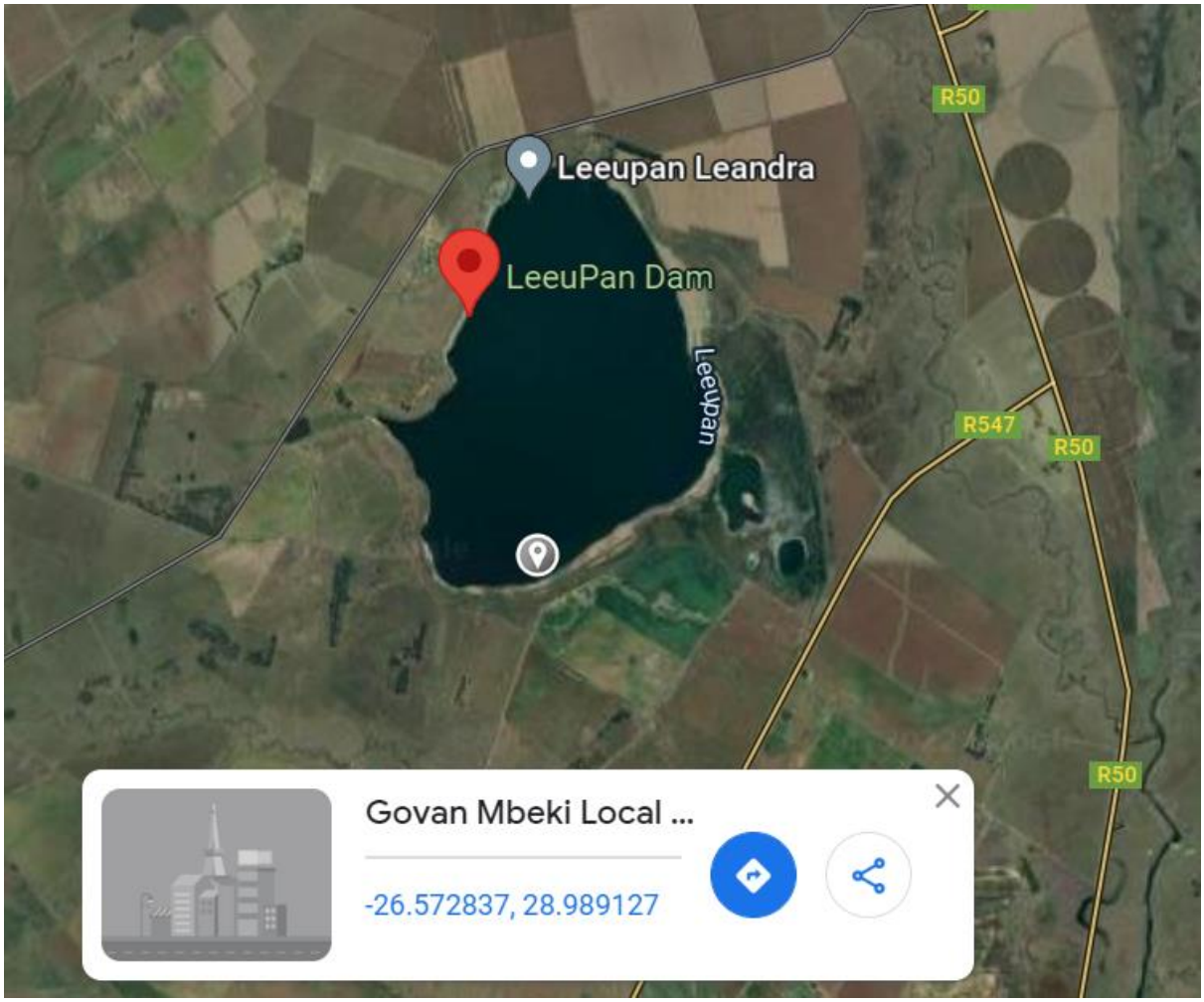

Figure 3. 6: Leeupan dam downstream of Evander Gold Mine, East Rand (Mpumalanga province).

Table 3. 1: Origin and description of samples in East Rand.

Sample matrix	Water and Sediment	Sample detail
Sample No.	Sample Area	Description of the sample area
1	Evander	Downstream of mining operations at Leeupan's dam (Recreational Site)
2	East Rand	Downstream of mining operations at Blesbok Spruit

Table 3. 2: Origin and description of samples in West Rand.

Sample matrix	Water and Sediment	Sample detail
Sample No.	Sample Area	Description of the sample area
1	Westonaria	Downstream of Peter Wright Dam Outflow
2	Krugersdorp	Water taken at Donaldson Dam Winze 17 and Winze 18, i.e., Underground water at pump station before Treatment Plant, Water from the treatment plant into the Spruit. Sediment taken at Donaldson Dam.

Table 3. 3: Origin and description of samples in Klerksdorp.

Sample matrix	Water and Sediment	Sample detail
Sample No.	Sample Area	Description of sample area
1	Carltonville	Deelkraal recreational dam
2	Klerksdorp	Bob Gardener dam

Table 3. 4: Origin and description of samples in Welkom.

Sample matrix	Water and Sediment	Sample detail
Sample No.	Sample Area	Description of the sample area
1	Theunessen	Blaauwdrift sand river downstream of mining operations
2	Welkom	Voelpan dam next to Nyakallong Township

Apparatus used in sampling

The collection of samples in different provinces and locations requires certain equipment to ensure safe collection and packaging. The locations of samples are seldom in remote areas and include water boreholes, streams passing beneath bridges, sediment near dams, etc. to collect such samples safely requires an individual to be positioned at a distance which guarantees safety for the person and allows for the collection of the sample. Apparatus were used in the collection of samples for this study, and they included the following:

- 2 litre plastic bottles
- Plastic tubs
- 60 litre cooler bag
- Spatula
- Rubber gloves
- 3 litres water bucket

Collection of samples was done with the use of a spatula; rubber gloves; water bucket; and plastic bottles for water samples, plastic tubs for sediments. Once collected, the samples were placed in a cooler bag to prevent contamination, cross-contamination, or damage to the sample

containers and seals. They were then transported to the Analytical Laboratory at the Centre for Applied Radiation Science and Technology (CARST) for analysis.

Apparatus used in the analysis of samples

- Canberra HPGe gamma spectrometer
- Marinelli beakers
- Concentrated nitric acid
- Alpha spectrometer

The method used for data analysis was as follows:

- Water and sediment samples were analysed with respect to the activity concentrations in water and specific activities in sediments for naturally occurring long-lived radionuclides of the decay chains of ^{238}U, ^{235}U, and ^{232}Th.
- Sediment samples were placed in containers closed with lids and sealed on the edges with Prestik to prevent air escape from the tub (Figure 3.7). The samples were then left to sit for 20 days. This was to allow the thorium and uranium daughter radionuclides to reach secular equilibrium (Vukanac et al., 2022). High-resolution gamma spectrometry (HRGS, Ge-detector with efficiency recorded to be $\geq 30\%$ with a resolution of ≤ 1.800 keV full width at half-maximum (FWHM) at 1.33 MeV and resolution ≤ 0.875 keV FWHM at 122 keV cooled by liquid nitrogen), with energy range 60 – 2070 keV and channel range 0 – 4095, was applied for all samples.
- Insoluble fractions were removed by filtering the water samples. The decay of radionuclides was prevented by treating the samples with 2 Molar concentrated nitric acid to pH 2 to annihilate biological activity, stabilize the samples, and prevent radionuclides from sticking onto the walls of the containers (Alkhomashi, 2016; Chen et al., 2021). 1 ml of ^{232}U tracer solution with an activity concentration of 107 mBq/g was used to spike 200 ml of the filtered sample, in a 400 ml glass beaker. Then a hot plate on a fume hood was used to evaporate the sample to a volume of 10 to 50 ml.

Lanthanide precipitation was used with the precipitation of test sources to prepare samples. Thereafter, the samples were analysed with alpha spectrometry (Vadja, 2012).

- Activity determination of radionuclides was done through the activity of their decay daughters. For example, ^{234}Pa was used to determine the activity of ^{238}U (Yücel et al., 1998).

Figure 3. 7: Sediment containers sealed with pre-stick.

Figure 3. 8: Bulk collected water samples and 200 ml container samples.

3.3 Energy calibration for the gamma spectrometer

The energy calibration of the gamma system was done with two apparatuses, namely the gamma-spectrometer system (complete with a processing computer and Genie-2000 software) and the radioactive source with a calibration certificate traceable to NIST, as can be seen in Table 3.5. Counting of the calibration test sample was set for a lifetime of 1800 seconds to produce clear and defined peaks, with calibration settings of energy in kilo-electron volts

(keV), tolerance units of full width at half-maximum (FWHM), tail curves set on low, and continuum of steps over four channels.

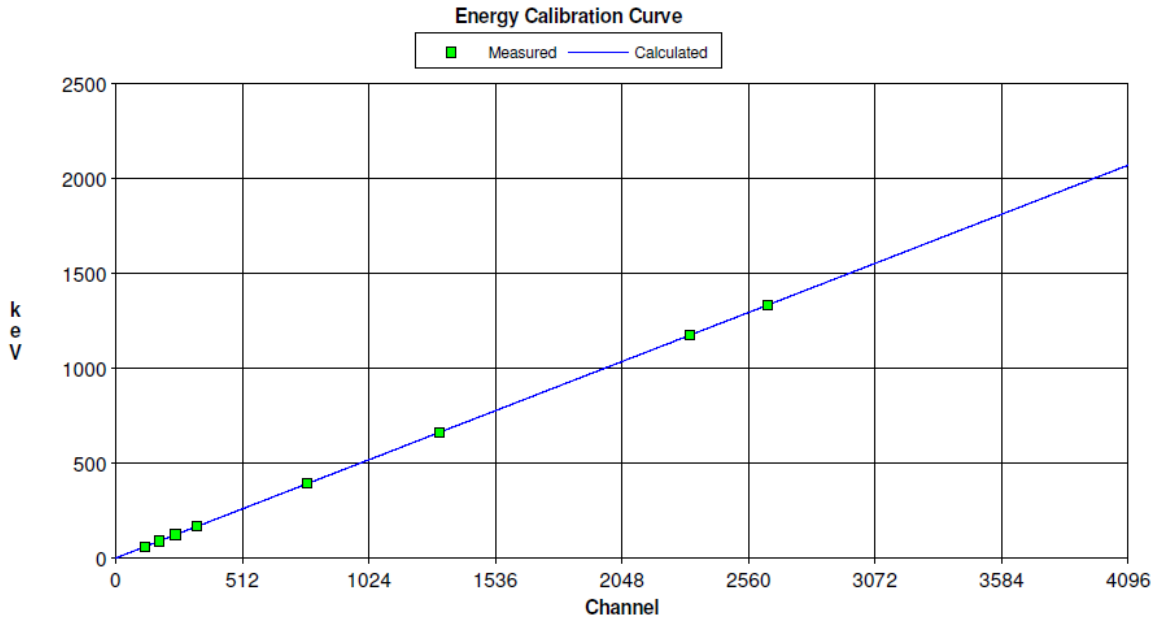

Figure 3. 9: Energy calibration curve for test source on the gamma spectrometer.

Figure 3.9 shows the linear relationship between the energy, measured in keV on the y-axis, and the channel number, on the x-axis.

3.4 Efficiency calibration for the gamma spectrometer

The efficiency calibration involved the germanium spectrometry system and the Laboratory Sourceless Calibration Software (LabSOCS) with geometry composer. The absolute photopeak efficiency is outlined in the following equation:

$$Efficiency(E_\gamma) = \frac{counts\ per\ second\ observed\ in\ the\ spectrum\ photopeak}{emitted\ gamma\ rays\ per\ second\ by\ the\ source} \quad [4]$$

The efficiency calibration process commenced with the input of the sample container dimensions. Then the geometry composer was run with a simplified beaker template selected. The detector was matched to the sample container, and then parameters of the geometry were

entered to describe the source and its relationship to the detector. Thereafter, the efficiency points (i.e., curve and parameters) were computed. Finally, the efficiency curve associated with a calibration with Genie 2000 was created wherein two curves for low and high energy were generated, as seen in Figure 3.10.

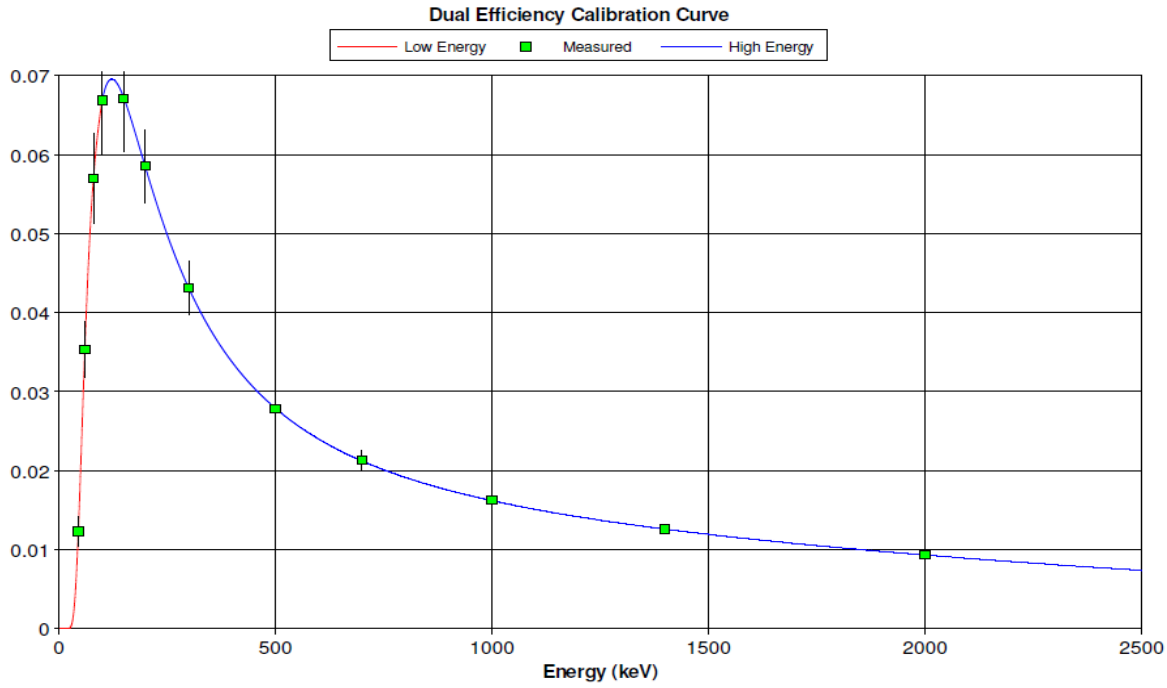

Figure 3. 10: Efficiency calibration curve for gamma spectrometer.

The relative efficiency calibration curve for the HPGe detector of the gamma spectrometer is shown in Figure 3.10. The distance between the source and the detector is maintained at 10cm to avoid summing (Sai et al., 2022).

3.5 Energy calibration of the alpha spectrometer

The energy calibration of the alpha system was done by counting a certified reference source attained from Eckert and Ziegler Analytics. The calibration of the alpha spectrometer was performed for each chamber using an alpha standard which was electro-deposited onto a source in the form of a stainless-steel disc containing mixed radionuclides. The radionuclides contained in the source were ^{241}Am, ^{238}U, ^{230}Pu, and ^{234}U, with energy ranges of 4.18 MeV to

5.47 MeV. The reported uncertainties were quoted at 2 sigma with a coverage factor k = 2, giving a 95% confidence level. The uncertainty budget included counting statistics, calibration source uncertainty, and sample geometry.

3.6 Counting Statistics

Good statistics are an important requirement in radiometric assessment. Counting statistics, in this context, means that the total gamma rays counted in a particular measurement must be large enough to be viewed as a statistically reliable. This is also related to the accuracy desired from a measurement (Chase & Rabinowitz, 1967; IAEA, 2003). Since radioactive decay is a random process, one standard deviation (σ) in a counting measurement is equal to the square root of the total count (n). This can be used to represent a percentage of the count or percentage error (Killeen et al., 2015). One standard deviation is represented by:

$$\sigma = \sqrt{n} \qquad [5]$$

Therefore, the error in measurement where n = 100 would be ±10 counts, equivalent to a percentage error of ±10%. Whereas a measurement where n = 1000 would give an error of ±31.6 counts, equivalent to a percentage error of ±3%.
The standard deviation in the counting rate can be calculated by:

$$\sigma_{RATE} = \sqrt{RATEt^{-1}} \qquad [6]$$

where $RATE = nt^{-1}$ is the counting rate.

When numerous corrections like background subtraction and spectrum stripping are applied, the error in the final result will increase because each correction has a counting measurement with its accompanying errors. The count must be increased in order to attain a smaller error, this can be done in one of three ways. Firstly, by counting for a longer period. Secondly, by increasing the size of the detector. Thirdly, placing the detector closer to the source (Killeen et al., 2015).

3.7 Analytical Methods and Instrumentation

Charged particle and gamma-ray energy spectrum measurements have been greatly streamlined and enhanced with the development of semiconductor detectors for the measurement of radioactivity. The most efficient solid-state detectors for spectral analysis are those made of silicon for alpha particles and germanium for gamma rays. Radiation is identified by its distinctive peak energy using spectral analysis, and its activity concentration is established using the count rate within the peak region of interest. The following equation can be used to calculate the activity concentration radionuclides of interest in the sample (Bakr, 2014):

$$A = \frac{1}{B.R.\gamma \times \eta\gamma \times t \times M} \times N s\gamma \qquad [7]$$

Whereby,

A - the radionuclide activity concentration in Bq/kg or Bq/L,
$B.R.\gamma$ – emission probability of the gamma line corresponding to the peak energy,
$\eta\gamma$ – efficiency corresponding to the peak energy (γ) at the specific geometry,
t – real counting time,
M – mass of the sample in kg or mL, and
$Ns\gamma$ – net count under the peak area of the selected gamma line for the measured sample.

Gamma-ray and alpha particle spectrometers use different detecting systems. As stated before, gamma detectors (crystals) are either p or n type and come in sizes of 10 to 12 cm. they are also created with minimal impurity levels. These crystals form the makeup of HPGe detectors. Germanium detectors have a low gap of the characteristic energy peak, which lessens interference from background radiation and other radionuclides in the sample. The detecting systems need extremely reliable power supplies and amplifiers to support analysis at high-energy resolution. A typical gamma-ray spectrometry system is made up of a preamplifier, amplifier, multichannel analyzer, high voltage power supply, computer, and specialized software, as well as an HPGe detector (typically a semiconductor or scintillator, such as NaI(Tl) or plastic scintillator) with lead shielding for background reduction. Using approved software programs like Genie 2000, the spectrometric system captures, saves, and processes the gamma-ray spectrum of the counted sample (Hodgson & Manus, 2006). The solid-state detectors

employed for alpha particles are silicon diodes, with an extremely thin, sensitive surface made of p-type silicon over a much thicker wafer of n-type silicon. A reliable power source applies a reverse bias of approximately 50V across the diode. As alpha particles hit the sensitive surface of the detector's n-type layer, they create electron-hole pairs that are directly proportional to the alpha particle's energy. A charge-sensitive preamplifier collects the pulse produced when the electron-hole pairs are propelled to the electrodes. After being amplified by an appropriate low-noise amplifier, the pulse is supplied into a multichannel pulse height analyser. The latter is merely a mechanism for categorizing incoming pulses according to their amplitude and storing them in the proper channels or bins that are linearly related to the energy (Hodgson & Manus, 2006). Figure 3.11 displays a schematic diagram of an alpha spectrometer and its components (Veale, 2009).

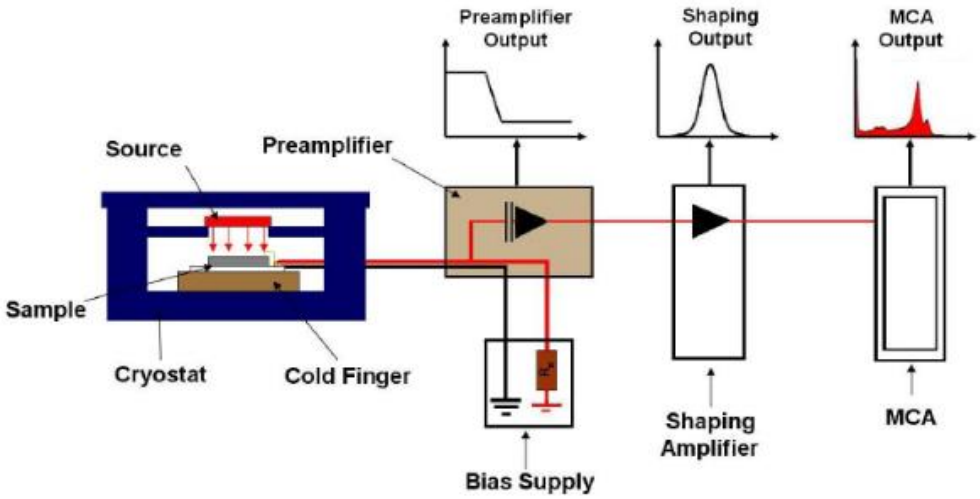

Figure 3. 11: Schematic diagram for alpha spectrometry.

A tiny silicon detector and a thin sample are put in a little vacuum chamber to prevent energy loss for alpha particles in the air. In most operations, shielding is unnecessary because alpha and beta semiconductor detectors are insensitive to gamma radiation. The chamber system shields background radiation other than alpha particles, which is not significantly detected in the thin solid. Nuclei with distinct energies that are distinctive to the source produce alpha particles. Depending on its nuclear characteristics, an alpha emitting radionuclide may emit alpha particles with a single discrete energy or a range of energies. The energy of the alpha particles was well characterized in both scenarios and can be utilized to describe the emitting

nuclide. The alpha energy spectra of suitable sources can be measured for qualitative and quantitative evaluations (Veale, 2009).

3.8 Determination of uranium in sediments

Determination of uranium in sediment was done using a Canberra gamma spectrometer high purity germanium (HPGe) detector, as depicted in Figure 3.12. The specifications of the instrument include the detector model GC3018, preamplifier model 2002CSL, crystotat model 7500SL, cryocooler model CCII-VD. The relative efficiency of the detector is recorded to be $\geq 30\%$ with a resolution of ≤ 1.800 keV FWHM at 1.33 MeV and resolution ≤ 0.875 keV FWHM at 122 keV. The multi-channel analyzer (MCA) used is 'Links.' Measured performance indicates 33.4% efficiency at 1332 keV.

Table 3. 5: Calibration sources for gamma spectrometry.

Nuclide	Gamma-ray energy (MeV)	Activity (kBq)	Emission rate (s^{-1})
Americium-241	0.060	3.40	1.22×10^3
Cadmium-109	0.088	15.8	0.577×10^3
Cobalt-57	0.122	0.562	0.481×10^3
Cerium-139	0.166	0.699	0.559×10^3
Mercury-203	0.279	1.40	1.14×10^3
Tin-113	0.392	2.42	1.57×10^3
Strontium-85	0.514	2.77	2.73×10^3
Caesium-137	0.662	2.72	2.31×10^3
Yttrium-88	0.898	5.11	4.80×10^3
Cobalt-60	1.173	3.25	3.24×10^3
Cobalt-60	1.333	3.25	3.25×10^3
Yttrium-88	1.836	5.11	5.07×10^3

Traceability complies with the requirements as set by the National Institute of Standards and Technology (NIST) under traceability of radioactive standards to the NIST (Montgomery, 1998).

Figure 3. 12: Sediment analysis with Canberra HPGe detector.

3.9 Determination of uranium in water

In the analysis of water samples, the instrumentation used included a semi-conductor silicon detector, a charge sensitive amplifier, and a linear amplifier, and data processing was done through a computer. The samples were placed in the Canberra alpha analyst chambers, as depicted in Figure 3.13, to be analysed. The source has an alpha emitter deposited on it, then placed at the bottom whilst the detector is placed above it. The source and detector are then placed inside a chamber with a vacuum, and a voltage of 100 volts is applied to the detector (Aggarwal, 2016; Guirguis et al., 2015).

Figure 3. 13: Alpha analyst chambers for water analysis.

The Eckert and Zeigler isotope products were used to calibrate the standard solution, with the source being ^{232}U (half-life of 68.9 years ± 1.0 years). A weighed aliquot solution was used to prepare the source for calibration. The activity of the solution (in µCi/g) was determined using gamma spectrometry. The peak energy of 583.2 keV was used for integration with the branching ratio of 0.306 gammas per decay. The concentration of the radionuclide was 0.7334 kBq/g.

Chapter 4: Results and Discussions

4.1 Uranium isotope activity concentration in sediments

Gamma spectra for sediment samples collected are displayed in Figures 4.1 and 4.2. The spectra were generated for all samples collected in North West, Mpumalanga, Free State, and Gauteng provinces. The activity of ^{238}U was determined through the detected ^{234m}Pa (Shazly et al., 2012; Vukanac et al., 2022). The isotopic ratios of all three isotopes were used to determine the activity for ^{234}U and ^{235}U (Walencik-Łata et al., 2021).

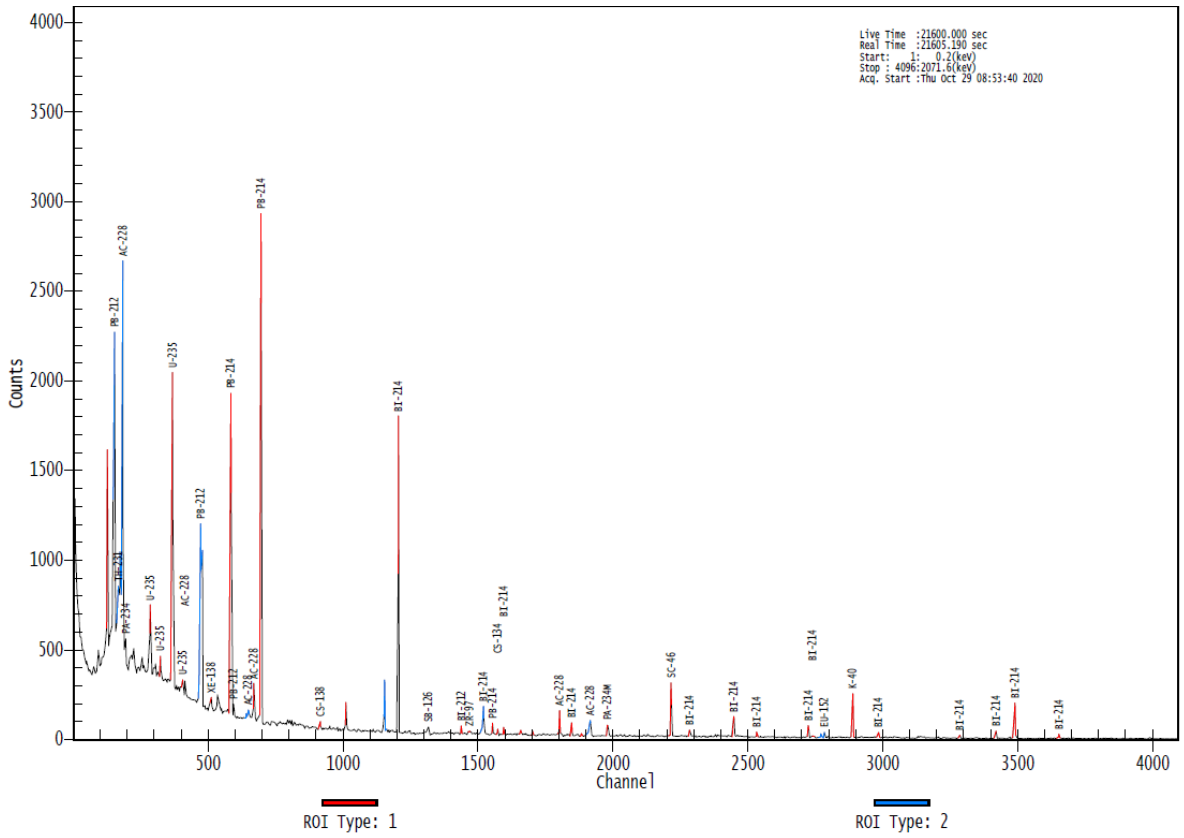

Figure 4. 1: Gamma spectrum of a samples collected from Mpumalanga Region.

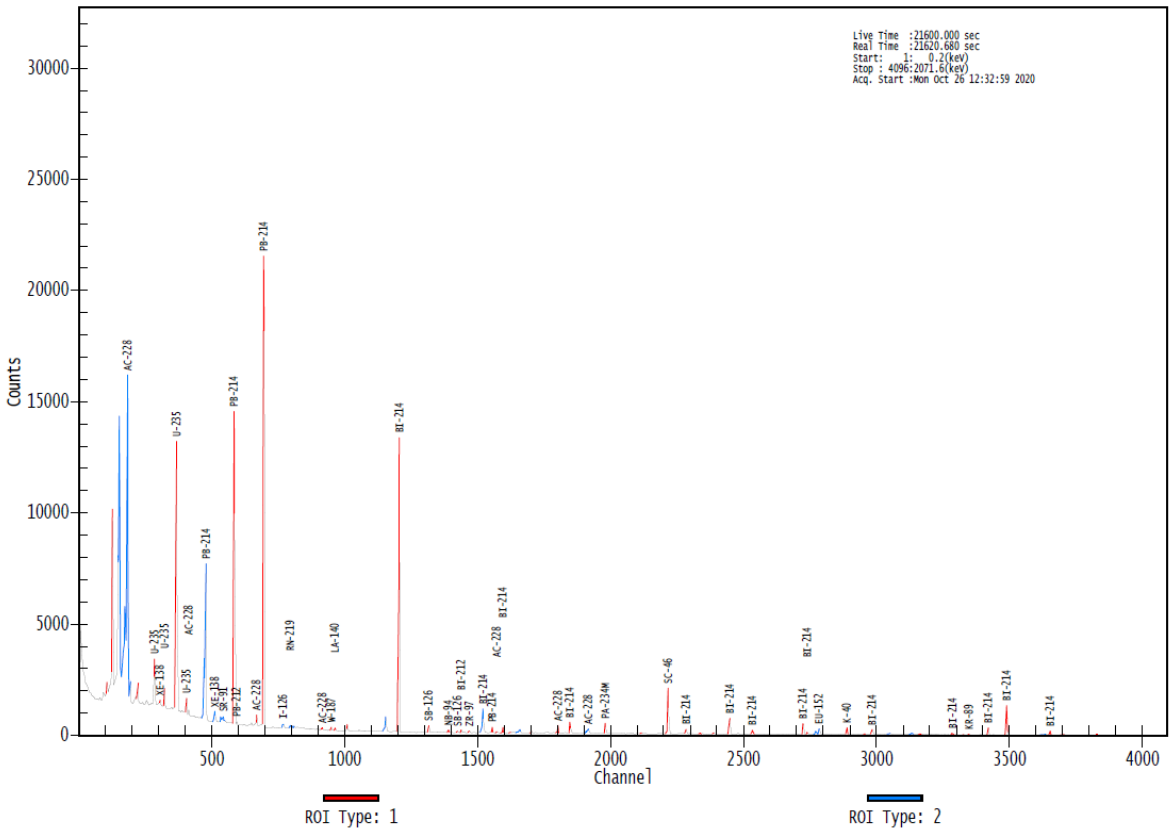

Figure 4. 2: Gamma spectrum of a samples collected from Gauteng region.

The energy level at which the element ^{234m}Pa peaked (approximately at channel 2000) is displayed in Figures 4.1 and 4.2. The energy line used for the spectrum in Figure 4.1 (herein referred to as sample 1, collected in Mzimhlophe location) was 1001.03 keV, corresponding to a ^{238}U activity value of 0.24 Bq/g. The spectrum in Figure 4.2 (sample 2, collected at Peter wright outlet dam) corresponded to a ^{238}U activity value of 2.54 Bq/g. The activities of isotopes for sample 1 were calculated as follows:

$$U-238=\frac{0.24Bq}{g}=240Bq/kg \quad [8]$$

$$U-234=\frac{0.24Bq}{g}\times 1.02=\frac{0.2448Bq}{g}=245Bq/kg \quad [9]$$

$$U-235=\frac{0.24Bq}{g}\times 0.048=\frac{0.01152Bq}{g}=11.52Bq/kg \quad [10]$$

Similar calculations were applied for sample 2 and the rest of the samples from the regions of interest. The results with uncertainties of 24 samples, where each of the four regions is represented by 6 samples, are presented in tables 4.1 to 4.4.

Table 4. 1: Uranium activity in sediment collected in Welkom.

Date collected	Welkom	^{238}U (Bq/kg)	^{235}U (Bq/kg)	^{234}U (Bq/kg)
Sep-20	Sample 1	70 ±32	3 ±2	71 ±33
	Sample 2	200 ±30	10 ±1	204 ±31
Dec-20	Sample 3	67 ±25	3 ±1	68 ±26
	Sample 4	452 ±46	22 ±2	461 ±47
Mar-21	Sample 5	215 ±29	10 ±1	219 ±30
	Sample 6	116 ±32	6 ±2	118 ±33

Table 4.1 indicates activity of samples collected on three different quarters of the year in Welkom. The highest activity was 461 Bq/kg for ^{234}U in December 2020, whilst the lowest activity was found to be 3 Bq/kg for ^{235}U September and December 2020. The uncertainty in some sample results e.g., sample 1 and sample 3 might be as a result of random and systematic uncertainties such as uncertainty in net count rates for the ^{235}U in the region of interest; moisture correction; calibration pad and sources (Amestoy et al., 2021; Davis, 2004).

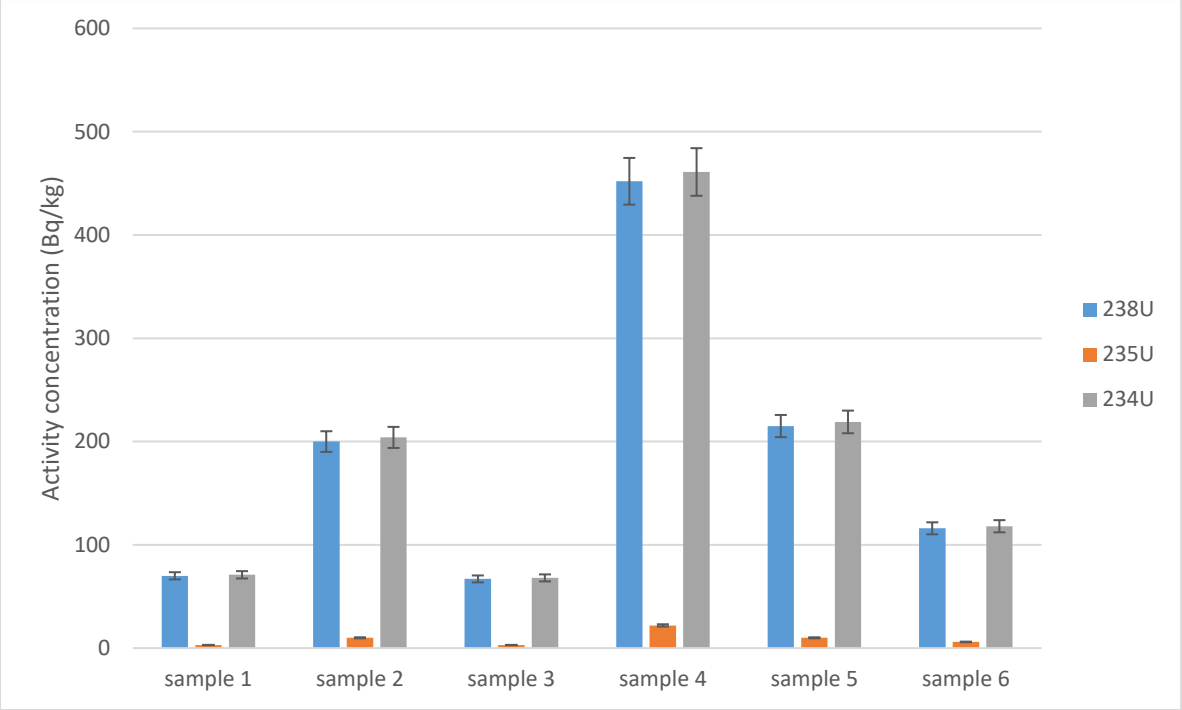

Figure 4. 3: Uranium activity graph of sediments collected in Welkom.

In figure 4.3, the highest activity concentration was 461 Bq/kg. This value is below the regulatory exclusion level of 500 Bq/kg set by the National Nuclear Regulator of South Africa (NNR). The activity concentration of all the samples indicates a general compliance with regulatory limits.

Table 4. 2: Uranium activity in sediment collected in Klerksdorp.

Date collected	Klerksdorp	^{238}U (Bq/kg)	^{235}U (Bq/kg)	^{234}U (Bq/kg)
Sep-20	sample 1	248 ±19	12 ±1	253 ±19
	sample 2	369 ±40	18 ±2	376 ±41
Dec-20	sample 3	578 ±72	28 ±3	590 ±73
	sample 4	297 ±30	14 ±1	303 ±30
Mar-21	sample 5	389 ±62	19 ±3	406 ±63
	sample 6	832 ±48	40 ±2	849 ±49

Table 4.2 indicates the activity concentration of uranium isotopes in samples collected on three different quarters of the year in Klerksdorp. The highest activity was 849 Bq/kg for ^{234}U in March 2021, whilst the lowest activity was found to be 12 Bq/kg for ^{235}U September 2020. An increasing trend in activity is observed for each radioisotope from September 2020 to March 2021.

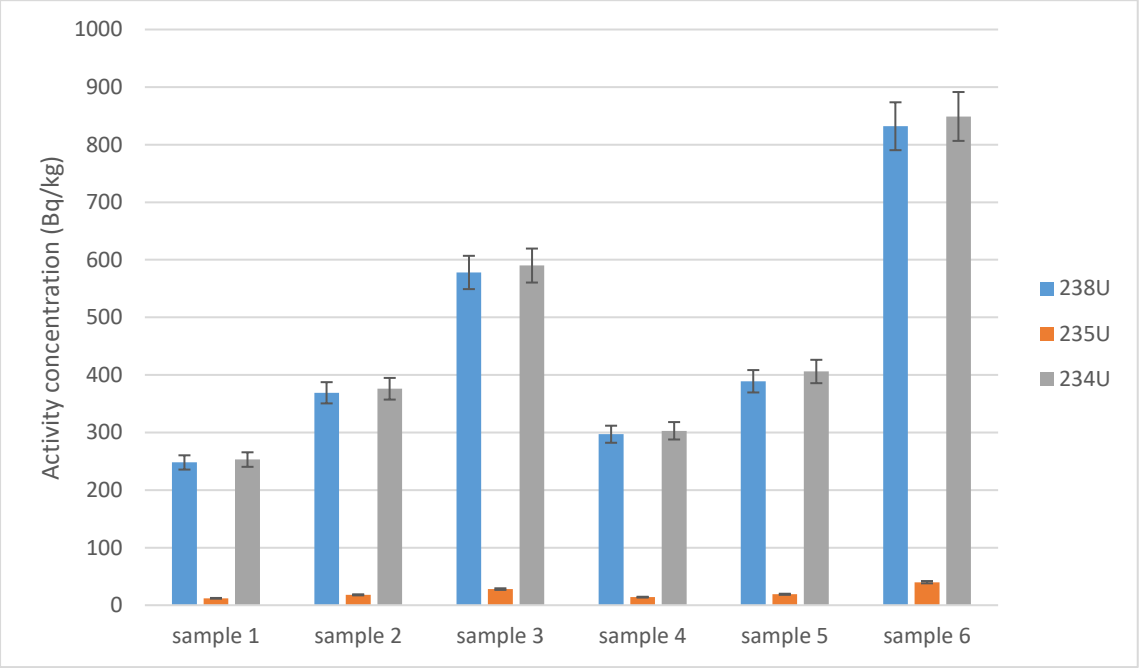

Figure 4. 4: Uranium activity graph of sediments collected in Klerksdorp.

The samples collected in Klerksdorp indicate some activity within regulatory limits. The highest value was 832 Bq/kg, which is above the 500 Bq/kg exclusion level set by the NNR. Figure 4.4 displays a relative increasing trend in activity from sample 1 to 6. The sample was collected near the currently non-operational Shiva Uranium Plant, which focused on the mining of uranium. This might be the reason for the high activity levels in the samples.

Table 4. 3: Uranium activity in sediment collected in West Rand.

Date collected	West Rand	^{238}U (Bq/kg)	^{235}U (Bq/kg)	^{234}U (Bq/kg)
Sep-20	sample 1	2550 ±165	122 ±8	2600 ±168
	sample 2	344 ±87	17 ±4	351 ±89
Dec-20	sample 3	6162 ±276	296 ±13	6285 ±282
	sample 4	400 ±105	19 ±5	408 ±107
Mar-21	sample 5	514 ±81	25 ±4	524 ±83
	sample 6	1260 ±104	60 ±5	1290 ±106

Table 4.3 indicates the activity concentration of uranium isotopes in samples collected on three different quarters of the year in West Rand. Here, there is significant activity of ^{234}U and ^{235}U in September 2020 and December 2020. The highest activity was 6285 Bq/kg for ^{234}U in December 2020, whilst the lowest activity was found to be 17 Bq/kg for ^{235}U September 2020.

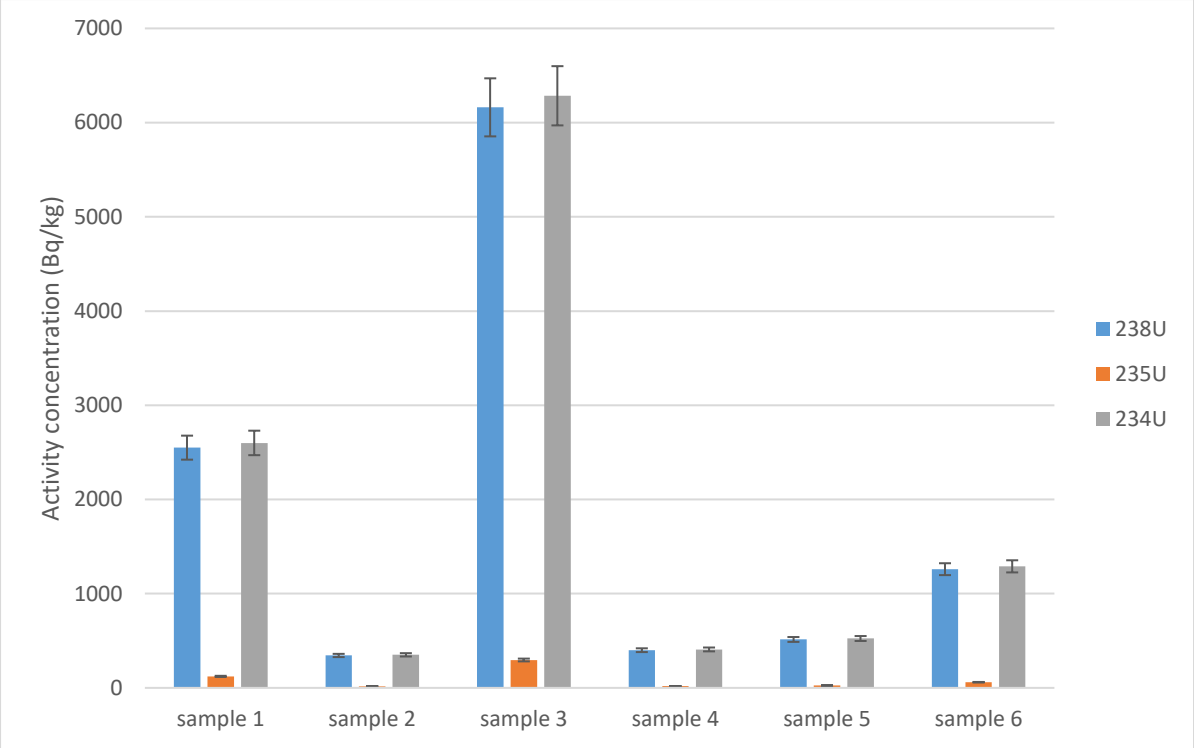

Figure 4. 5: Uranium activity graph of sediments collected in West Rand.

Figure 4.5 displays the samples collected in West Rand from September 2020 to March 2021. Although some activity concentrations were below the regulatory exclusion limit of 500 Bq/kg, the highest value was 6285 Bq/kg, which is above the exclusion limit. A significant jump in activity from sample 3 can be in figure 4.5. The significance of this activity concentration could not be verified because the pre-existing background radioactivity levels are unknown.

Table 4. 4: Uranium activity in sediment collected in East Rand.

Date collected	East Rand	^{238}U (Bq/kg)	^{235}U (Bq/kg)	^{234}U (Bq/kg)
Sep-20	sample 1	86 ±33	4 ±2	88 ±34
	sample 2	240 ±44	12 ±2	245 ±45
Dec-20	sample 3	434 ±43	21 ±2	442 ±44
	sample 4	96 ±24	5 ±1	98 ±24
Mar-21	sample 5	189 ±38	9 ±2	193 ±39
	sample 6	516 ±150	25 ±7	526 ±153

Table 4.4 indicates the activity concentration of uranium isotopes in samples collected on 3 different quarters of the year in East Rand. Here, there is relatively low activity which is below exclusion levels of 500 Bq/kg. The highest activity was 526 Bq/kg for ^{234}U in March 2021, whilst the lowest activity was found to be 4 Bq/kg for ^{235}U September 2020.

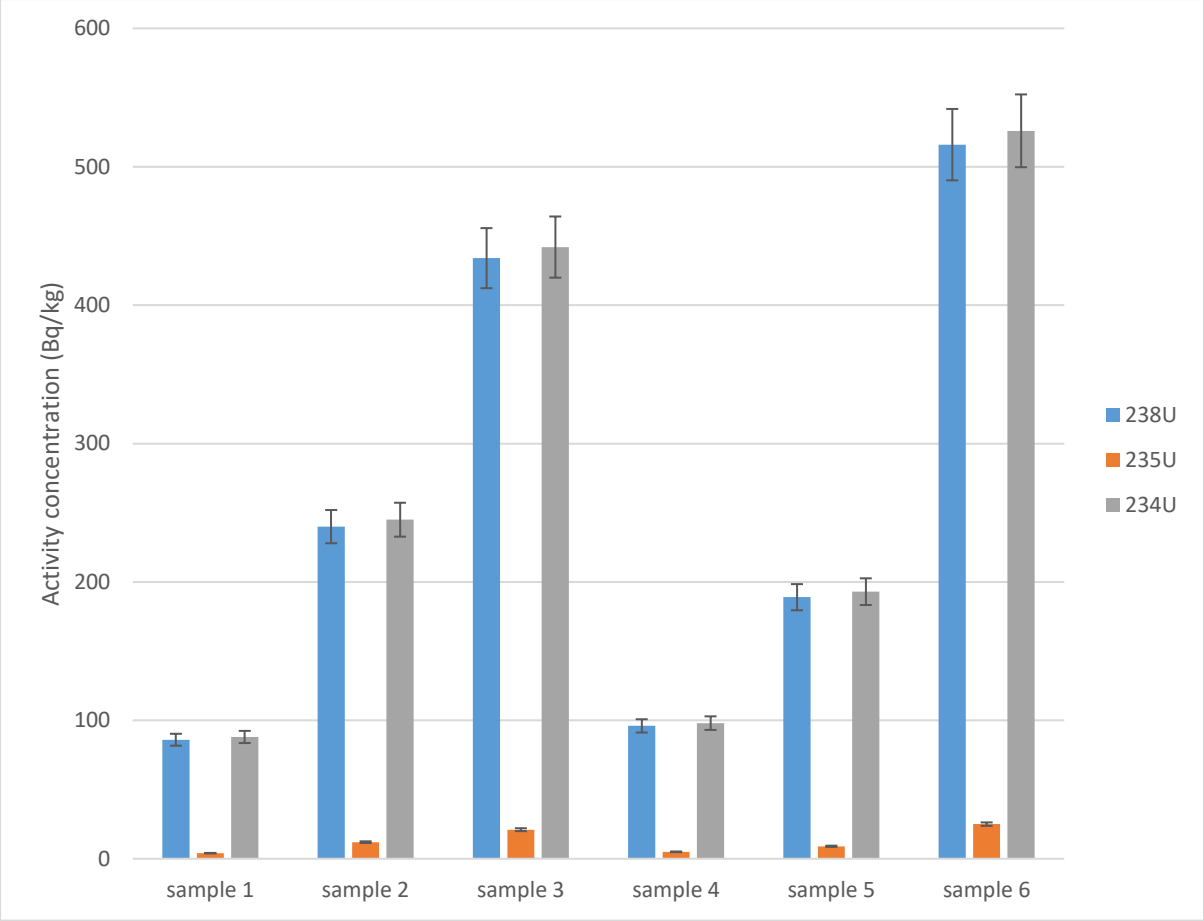

Figure 4. 6: Uranium activity graph of sediments collected in East Rand.

Figure 4.6 displays the samples collected in East Rand from September 2020 to March 2021. Although activity concentrations fluctuate from sample 1 to sample 6, the general trend is that activity concentrations were below the regulatory exclusion limit.

4.2 Uranium isotope activity concentration in water

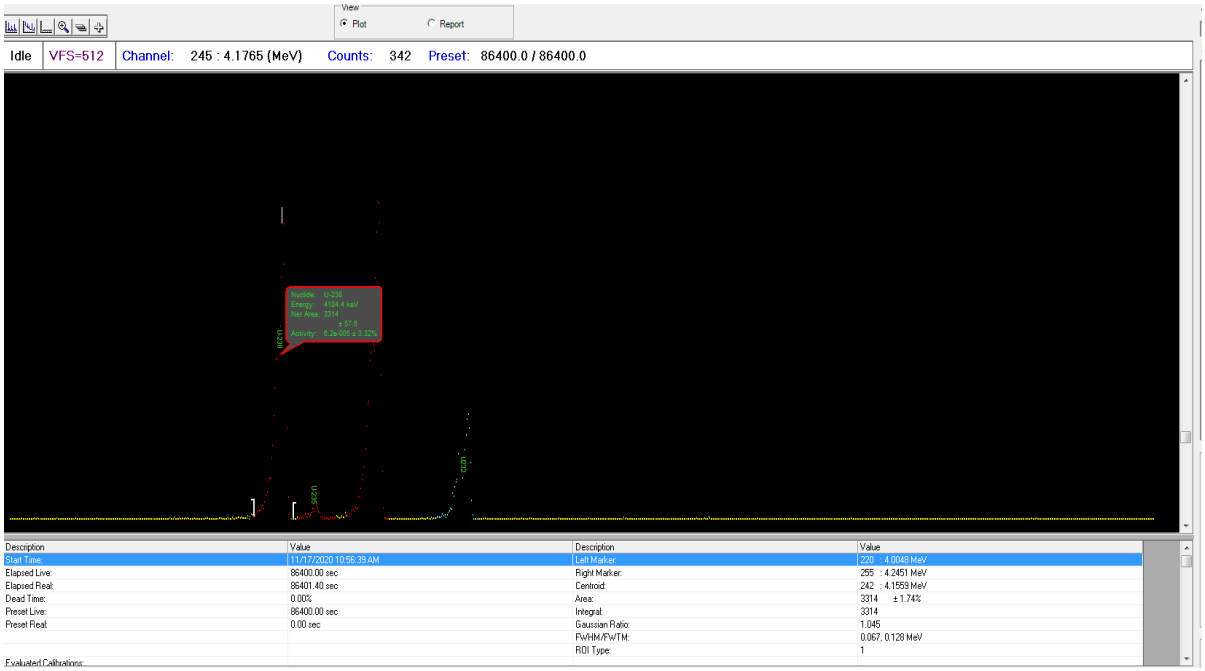

Figure 4. 7: Spectrum of a water sample collected in Klerksdorp.

Figure 4.7 indicates a spectrum of counts (represented on the y-axis) versus channel (represented on the x-axis) and displays four peaks which identify the radionuclides involved and the tracer. The first peak represents ^{238}U, the second peak is for ^{235}U, the third peak is for ^{234}U, and the fourth peak represents the ^{232}U tracer. The red-framed box on the spectrum gives information on the peak i.e., the nuclide (^{238}U); the energy (4184.4 keV); the net area (3314 ±57.6); and the activity ($6.2 \times 10^{-5} \pm 3.32\%$). Similarly, the peaks in figure 4.8 also represent these radionuclides in the same order.

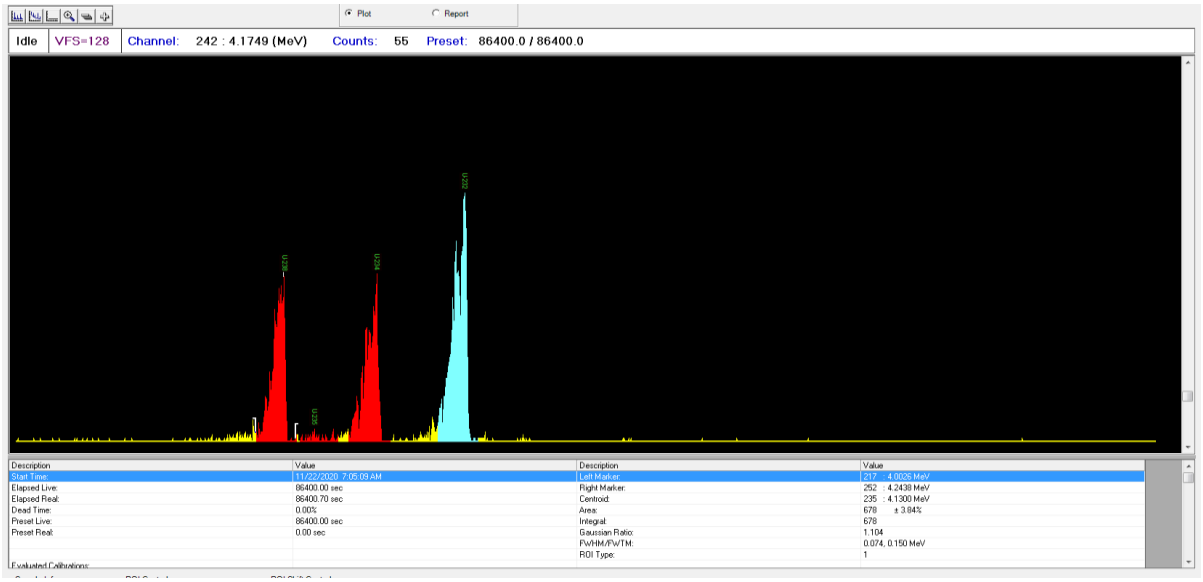

Figure 4. 8: Spectrum of water sample collected in Welkom.

The activity of water samples in the different regions was observed from generated spectrums. Figures 4.7 and 4.8 show examples of the display of counts (on the y-axis) and channels (on the x-axis) for ^{238}U, ^{235}U, ^{234}U, and the tracer ^{232}U from different water samples collected in Klerksdorp and Welkom. It was observed from the two figures that the ^{238}U isotope peaked at the same channel range (i.e., Channel 242 to 245) with the same energy of 4.17 MeV. Similar spectra were generated for all other water samples.

The results of activity concentration of ^{238}U, ^{235}U, and ^{234}U with their uncertainties in 24 samples, where each of the four regions represented by 6 samples, are presented in Tables 4.5 to Table 4.8.

Table 4. 5: Water samples collected in the East Rand.

Date collected	East Rand	^{238}U (mBq/L)	^{235}U (mBq/L)	^{234}U (mBq/L)
Mar-21	Sample 1	667 ±19,81	26 ±3,33	690 ±20,07
	Sample 2	236 ±10,58	6 ±1,08	231 ±10,36
Sep-20	Sample 3	714 ±18,49	33 ±3,97	686 ±18,12
	Sample 4	2435 ±35,06	106 ±7,29	2439 ±35,11
Dec-20	Sample 5	700 ±18,19	26 ±3,42	691 ±18,11
	Sample 6	91 ±6,81	3 ±1,1	99 ±7,09

Table 4.5 indicates activity concentration in water samples collected in the East Rand from September 2020 to March 2021. The highest activity was observed to be 2439 mBq/L for ^{234}U in September 2020, whilst the lowest activity was 3 mBq/L for ^{235}U in December 2020.

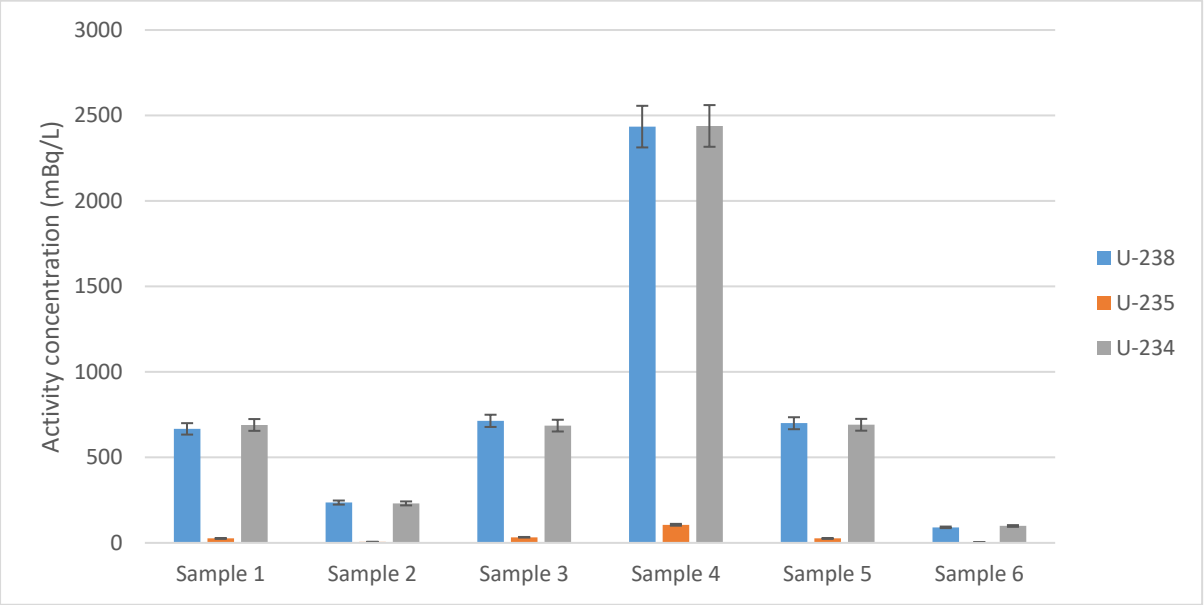

Figure 4. 9: Nuclide activity in water samples from the East Rand.

Figure 4.9 corresponds to the results in table 4.5, where the highest activity is observed at sample 4 collected in September 2020, peaking above the rest of the samples in activity. Sample

6 is also clearly represented as corresponding to the 3 mBq/L in table 4.5 as the lowest activity concentration.

Table 4. 6: Water samples collected in the West Rand.

Date collected	West Rand	^{238}U (mBq/L)	^{235}U (mBq/L)	^{234}U (mBq/L)
Mar-21	Sample 1	975 ±21,75	50 ±4,69	959 ±21,49
	Sample 2	13674 ±86,15	707 ±19,51	14968 ±89,81
Sep-20	Sample 3	1148 ±23,43	45 ±4,61	1189 ±23,79
	Sample 4	1171 ±23,54	46 ±4,64	1152 ±23,27
Dec-20	Sample 5	1126 ±22,29	48 ±4,57	1102 ±22,03
	Sample 6	25489 ±150,39	1218 ±32,88	28195 ±157,89

Table 4.6 indicates activity concentration in water samples collected in the West Rand from September 2020 to March 2021. The highest activity was observed to be 28195 mBq/L for ^{234}U in December 2020, whilst the lowest activity was 45 mBq/L for ^{235}U in September 2020. The ^{235}U activity is lowest in sample 1,3,4 and 5. This is generally expected since ^{234}U is the most soluble of the isotopes in water as explained in section 2.4.

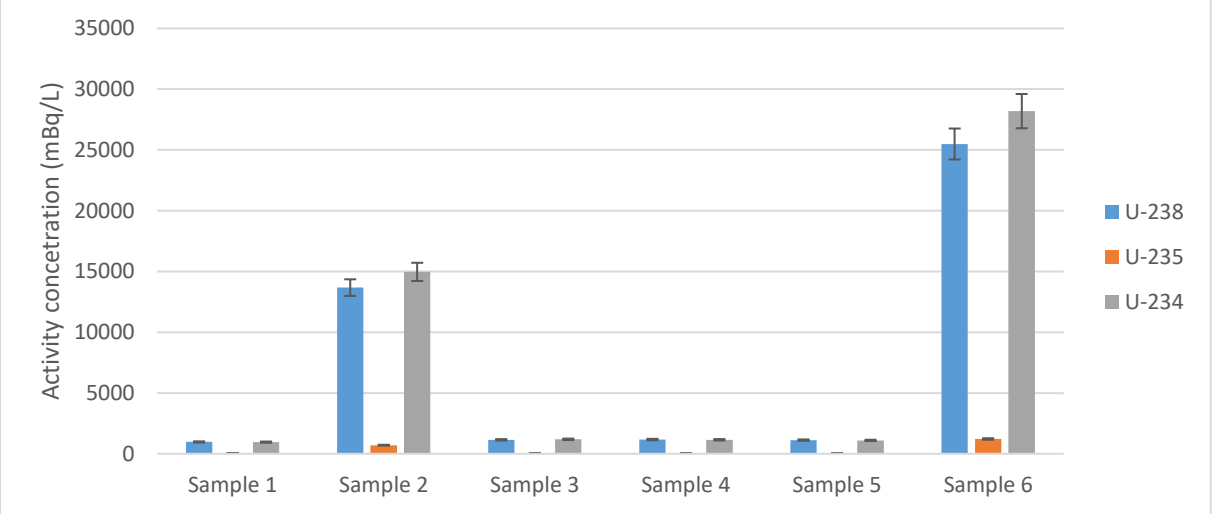

Figure 4. 10: Nuclide activity in water samples collected in the West Rand.

Figure 4.10 corresponds to the results in table 4.6, where the highest activity is observed at sample 6 collected in December 2020, peaking above the rest of the samples in activity. The rest of the samples are also clearly represented to be relatively low except for sample 2 which indicated the second highest activity in table 4.6 as well. The significant increase for sample 2 and sample 6 could be due to the discharge schedule of process water from mining operations near Peter Wright Dam.

Table 4. 7: Water samples collected in Welkom.

Date collected	Welkom	^{238}U (mBq/L)	^{235}U (mBq/L)	^{234}U (mBq/L)
Mar-21	Sample 1	1936 ±31,56	80 ±6,17	1993 ±32,09
	Sample 2	1801 ±31,87	77 ±6,32	1790 ±31,67
Sep-20	Sample 3	2008 ±35,33	164 ±10,08	2109 ±36,28
	Sample 4	1391 ±26,71	64 ±5,74	1387 ±26,77
Dec-20	Sample 5	4834 ±50,76	192 ±10,02	4771 ±50,09
	Sample 6	2106 ±45,49	94 ±9,4	2048 ±44,86

Table 4.7 indicates activity concentration in water samples collected in Welkom from September 2020 to March 2021. The highest activity was observed to be 2109 mBq/L for ^{234}U in September 2020, whilst the lowest activity was 64 mBq/L for ^{235}U in September 2020.

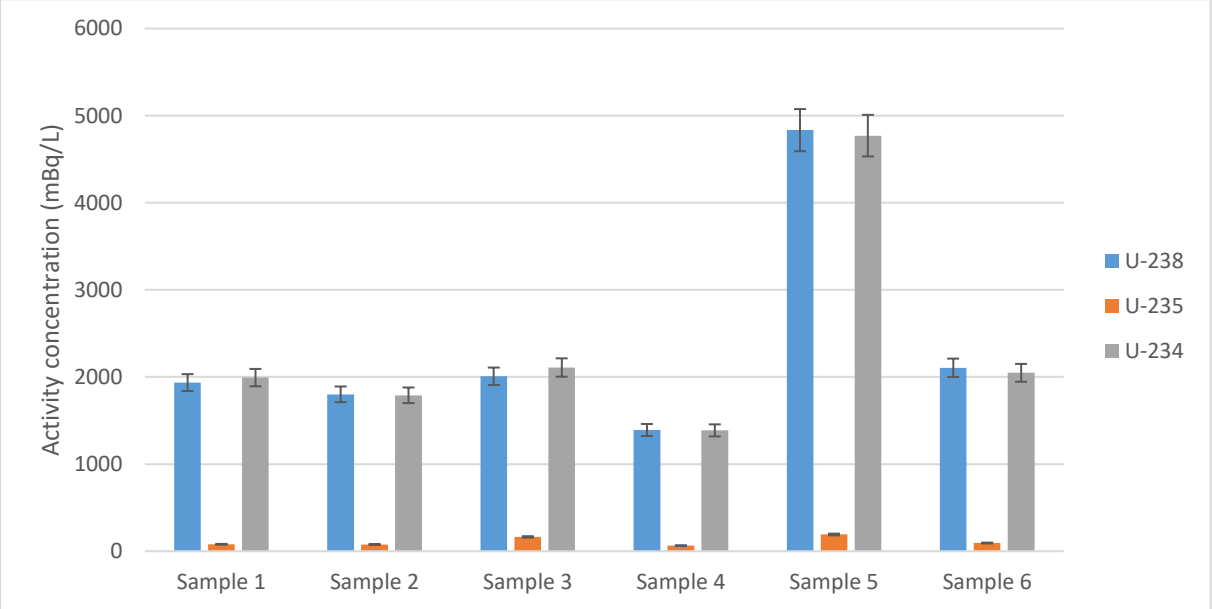

Figure 4. 11: Nuclide activity in water samples collected in Welkom.

Figure 4.11 corresponds to the results in table 4.7, where the highest activity is observed at sample 5 collected in September 2020, peaking above the rest of the samples in activity.

The rest of the samples are also clearly represented to be similar in activity throughout the months, displaying activities which are bordering the 2000 mBq/L for ^{234}U and ^{238}U whilst ^{235}U still has the lowest activity in all samples over the months.

Table 4. 8: Water samples collected in Klerksdorp

Date collected	Klerksdorp	^{238}U (mBq/L)	^{235}U (mBq/L)	^{234}U (mBq/L)
Mar-21	Sample 1	1058 ±23,38	44 ±4,33	1102 ±23,8
	Sample 2	1485 ±28,06	67 ±5,62	1575 ±28,98
Sep-20	Sample 3	3127 ±54,41	109 ±10,14	3574 ±57,89
	Sample 4	1312 ±25,19	52 ±4,95	1379 ±25,78
Dec-20	Sample 5	1299 ±25,21	39 ±4,33	1450 ±26,53
	Sample 6	3045 ±37,46	119 ±7,37	3554 ±40,52

Table 4.8 indicates activity concentration in water samples collected in Klerksdorp from September 2020 to March 2021. The highest activity was observed to be 3574 mBq/L for ^{234}U in September 2020, whilst the lowest activity was 39 mBq/L for ^{235}U in December 2020.

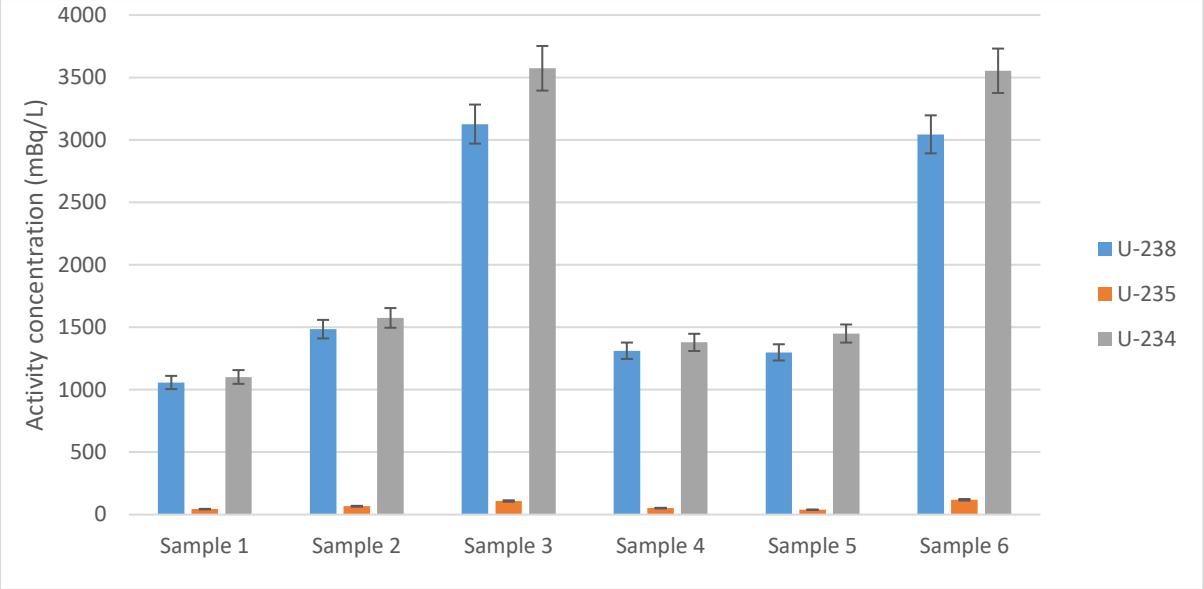

Figure 4. 12: Nuclide activity concentration in water samples from Klerksdorp.

Figure 4.12 represents the results in table 4.8, where high activity of almost the same concentration is observed at sample 3 collected in September 2020 and sample 6 collected in December 2020. This sample was collected from Bob Gardner Dam next to uranium mining operations (which are currently not taking place). The rest of the samples are also clearly represented to be similar in activity throughout the months, displaying activities which are bordering the 1500 mBq/L for ^{234}U and ^{238}U whilst ^{235}U continues to have the lowest activity in all samples over the months.

4.3 Distribution coefficient and uranium ratio in water

The distribution coefficient of uranium in water and sediment was calculated for samples in the 4 regions using equation [1]. Calculations for the distribution coefficient between 2 samples (1 water and 1 sediment) from the four regions, Klerksdorp, Welkom, East Rand, and West Rand are demonstrated in equation [12]-[15]. The distribution coefficient for each sample is presented in Table 4.9.

Klerksdorp:

$$K_d = \frac{C_s}{C_1} = \frac{[U^{238}+U^{235}+U^{234}]mBg/g}{[U^{238}+U^{235}+U^{234}]mB/L} = \frac{[389+19+406]mBg/g}{[1058+44+1102]mBq/L} = 0{,}3693 g.L^{-1} \quad [12]$$

Welkom:

$$K_d = \frac{C_s}{C_1} = \frac{[U^{238}+U^{235}+U^{234}]mBg/g}{[U^{238}+U^{235}+U^{234}]mB/L} = \frac{[215+10+219]mBg/g}{[1936+80+1993]mBq/L} = 0{,}1107 g.L^{-1} \quad [13]$$

West Rand:

$$K_d = \frac{C_s}{C_1} = \frac{[U^{238}+U^{235}+U^{234}]mBg/g}{[U^{238}+U^{235}+U^{234}]mB/L} = \frac{[514+25+524]mBg/g}{[975+50+959]mBq/L} = 0{,}5358 g.L^{-1} \quad [14]$$

East Rand:

$$K_d = \frac{C_s}{C_1} = \frac{[U^{238}+U^{235}+U^{234}]mBg/g}{[U^{238}+U^{235}+U^{234}]mB/L} = \frac{[189+9+193]mBg/g}{[667+26+690]mBq/L} = 0{,}2827 g.L^{-1} \quad [15]$$

Table 4. 9: Distribution coefficient (K_d) of uranium in sediment and water.

Region	Samples	Mar-21	Dec-20	Sep-20
		K_d ($g.L^{-1}$)		
Welkom	Sample 1	0,11	0,01	0,03
	Sample 2	0,07	0,22	0,15
Klerksdorp	Sample 1	0,37	0,43	0,08
	Sample 2	0,55	0,09	0,28
West Rand	Sample 1	0,54	5,6	2,21
	Sample 2	0,09	0,02	0,3
East Rand	Sample 1	0,28	0,63	0,12
	Sample 2	2,26	1,03	0,1

The distribution of radionuclides between solid and liquid phases influences their migration rate (Payne et al., 2011). The distribution coefficient K_d gives the ratio of the radionuclide concentration in sediment (C_s) to its concentration in water (C_1). The calculation of K_d in the four regions of interest indicated a low distribution of radionuclide from sediment to water for most of the regions as indicated in table 4.9. The highest distribution coefficient calculated was 5,60 $g.L^{-1}$ in the West Rand and the lowest was 0,01 g.L-1 in Welkom, both samples collected in the December 2020 period.

4.4 Ratio of $^{234}U/^{238}U$ in water samples

The ratio of radionuclide isotopes of uranium was calculated for the four regions. The samples collected in March 2021 were selected to demonstrate the ratios and Table 4.10 indicates the values calculated. An example is shown in equation [16]:

$$\frac{U^{234}}{U^{238}} = \frac{1102 mBq/L}{1058 mBq/L} = 1{,}0416 \qquad [16]$$

Table 4. 10: Ratio values of $^{234}U/^{238}U$ water samples.

Region	Samples	Mar-21	Dec-20	Sep-20
		$^{234}U/^{238}U$		
Welkom	Sample 1	1,03	0,99	1,05
	Sample 2	0,99	0,97	1
Klerksdorp	Sample 1	1,04	1,12	1,14
	Sample 2	1,06	1,17	1,05
West Rand	Sample 1	0,98	0,98	1,04
	Sample 2	1,09	1,11	0,98
East Rand	Sample 1	1,03	0,99	0,96
	Sample 2	0,98	1,09	1

The ratios in Table 4.10 ranged from 0,96 to 1,14, with an average of 1,01 in Welkom; 1,10 in Klerksdorp; 1,03 in West Rand; and 1,01 in East Rand. Radioisotopes which are formed by the decay of ^{238}U in crystalline mineral phase experiences recoil forces. The daughter nuclide ^{234}U is oxidized into the hexavalent stage once its parent nuclide Thorium-234 (^{234}Th) moves out of its crystal lattice, this enables ^{234}U to be more soluble in water than ^{238}U (Krachler et al., 2018). This then causes activity ratios of $^{234}U/^{238}U$ to be more than 1 in natural waters (Borylo & Skwarzec, 2014; Zielinski et al., 2000) and the ratios in groundwater to be 20 and more (Carvalho & Fajgelj, 2013). The ratios are thus in the expected range for natural waters. This is an indication that activity concentrations found for water and sediment are not significantly hazardous.

Chapter 5: Conclusions

The uranium concentration and its partitioning in sediment and water in different surface water bodies around mining operations in different regions of various provinces in South Africa have been determined. A total of 48 samples, including water and sediment samples were collected and analysed. Alpha and gamma spectroscopy were used as analysing methods described in Sections 2.7.1 and 2.7.4 for the detection of ^{238}U, ^{235}U, and ^{234}U and their activity concentrations. The following conclusions can be made from the results of the analysed samples:

- The highest concentration of ^{238}U, ^{235}U, and ^{234}U in water was found to be in the West Rand. The activity concentration for ^{238}U ranged from 975 mBq/L to 25489 mBq/L. The activity concentration for ^{235}U ranged from 45mBq/L to 1218 mBq/L and that of ^{234}U ranged from 959 mBq/L to 28195 mBq/L.
- The highest concentration of ^{238}U, ^{235}U, and ^{234}U in sediment was also found to be in the West Rand. The concentration for ^{238}U ranged from 344 Bq/kg to 6162 Bq/kg. The activity concentration for ^{235}U ranged from 17 Bq/kg to 296 Bq/kg and that of ^{234}U ranged from 351 Bq/kg to 6285 Bq/kg.
- The high concentrations found in the West Rand are due to released process water from mining operations. The samples were taken at the Peter Wright outlet dam. The increase in concentration can be seen in the results from September 2020 to December 2020 at this sampling point. However, a significant drop was also observed in March 2021 possibly from the rainy season which will impact some level of dilution in concentration.
- The ratio of $^{234}U/^{238}U$ for the samples collected ranged from 0,96 to 1,14. This is indicative of the similar characteristics in contamination due to the shared gold bearing basin of the Witwatersrand by the 4 regions under study as described in section 2.1.

References

Abiye, T., & Shaduka, I. (2017). Radioactive Seepage through Groundwater Flow from the Uranium Mines, Namibia. *Hydrology*, *4*(1), 11.

Aggarwal, S. (2016). Alpha-particle spectrometry for the determination of alpha emitting isotopes in nuclear, environmental and biological samples: past, present and future. *Analytical Methods*, 5353-5371.

Ali, M., Sadhu, B., Boda, A., Tiwari, N., Das, A., Musharaf Ali, S. K., Bhattacharya, D., Pandey, B. N., & Kumar, A. (2019). Thorium decorporation efficacy of rationally-selected biocompatible compounds with relevance to human application. *Journal of Hazardous Materials*, *365*, 952-961. https://doi.org/https://doi.org/10.1016/j.jhazmat.2018.11.038

Ali, M. Y. M., Hanafiah, M. M., & Khan, M. F. (2018). Potential factors that impact the radon level and the prediction of ambient dose equivalent rates of indoor microenvironments. *Science of The Total Environment*, *626*, 1-10. https://doi.org/https://doi.org/10.1016/j.scitotenv.2018.01.080

Alkhomashi, N. (2016). Determination of natural radioactivity in irrigation water wells in northwestern Saudi Arabia. *Chemosphere*, 1928-1936.

Amestoy, J., Meslin, P.-Y., Richon, P., Delpuech, A., Derrien, S., Raynal, H., Pique, É., Baratoux, D., Chotard, P., Van Beek, P., Souhaut, M., & Zambardi, T. (2021). Effects of environmental factors on the monitoring of environmental radioactivity by airborne gamma-ray spectrometry. *Journal of Environmental Radioactivity*, *237*, 106695. https://doi.org/https://doi.org/10.1016/j.jenvrad.2021.106695

Armstrong, R. A., Compston, W., Retief, E. A., Williams, I. S., & Welke, H. J. (1991). Zircon ion microprobe studies bearing on the age and evolution of the Witwatersrand triad. *Precambrian Research*, *53*(3), 243-266. https://doi.org/https://doi.org/10.1016/0301-9268(91)90074-K

Bakr, F. W. (2014). Analytical Method Validation of Gamma Spectrometric Procedure for the Determination of γ-Emitters in Environmental Samples. *Arab Journal of Nuclear Sciences and Applications*, *47*(3), 130-138. http://inis.iaea.org/search/search.aspx?orig_q=RN:45105958

Bangotra, P., Sharma, M., Mehra, R., Jakhu, R., Singh, A., Gautam, A. S., & Gautam, S. (2021). A systematic study of uranium retention in human organs and quantification of radiological and chemical doses from uranium ingestion. *Environmental Technology & Innovation*, *21*, 101360. https://doi.org/https://doi.org/10.1016/j.eti.2021.101360

Borylo, A., & Skwarzec, B. (2014). Activity disequilibrium between ^{234}U and ^{238}U isotopes in natural environment. *Journal of Radioanalytical and Nuclear Chemistry*, 719-727.

Brugge, D., & Buchner, V. (2011). Health effects of uranium: new research findings. *Review on Environmental Health*, 231-249.

Burnett, W., & Elzerman, A. (2001). Nuclide migration and the environemental radiochemistry of Florida phosphogypsum. *Journal of Environmental Radioactivity* 27-51.

Carvalho, F., & Fajgelj, A. (2013). Radioactivity in drinking water: routine monitoring and emergency response. *Water, Air, & Soil Pollution*, 1597.

Catuneanu, O. (2001). Flexural partitioning of the Late Archaean Witwatersrand foreland system, South Africa. *Sedimentary Geology*, *141-142*, 95-112. https://doi.org/https://doi.org/10.1016/S0037-0738(01)00070-7

Chambers, D. B., Cassaday, V. J., & Lowe, L. M. (1989). Exposures from mining and mine tailings. *International Journal of Radiation Applications and Instrumentation. Part C. Radiation Physics and Chemistry*, *34*(2), 295-307. https://doi.org/https://doi.org/10.1016/1359-0197(89)90237-3

Chase, G. D., & Rabinowitz, J. L. (1967). Principles of radioisotope methodology.

Chen, L., Zhang, J., Huang, Y., Peng, C., Chen, Y., Lu, L., Wang, X., & Wei, Y. (2021). An anion exchange pretreatment method for the determination of low-level uranium in the environmental water samples. *Journal of Environmental Radioactivity*, *237*, 106699. https://doi.org/https://doi.org/10.1016/j.jenvrad.2021.106699

Choppin, G., Liljenzin, J.-O., Rydberg, J., & Ekberg, C. (2013). Chapter 13 - Cosmic Radiation and Radioelements in Nature. In G. Choppin, J.-O. Liljenzin, J. Rydberg, & C. Ekberg (Eds.), *Radiochemistry and Nuclear Chemistry (Fourth Edition)* (pp. 373-404). Academic Press. https://doi.org/https://doi.org/10.1016/B978-0-12-405897-2.00013-6

Coetzee, H., Winde, F., & Wade, P. (2006). *Assessment of sources, pathways, mechanisms, and risks of current and potential future pollution of water and sediments in gold-mining areas of the wonderfonteinspruit catchment*.

Cole, D. (1998). Uranium. In *The mineral resources of South Africa: Handbook* (pp. 642-652). Council for Geoscience.

Creff, G., Zurita, C., Jeanson, A., Carle, G., Vidaud, C., & Auwer, C. D. (2019). What do we know about actinides-proteins interactions? *Radiochimica Acta*, *107*(9-11), 993-1009. https://doi.org/doi:10.1515/ract-2019-3120

Cresswell, T., Metian, M., Fisher, N. S., Charmasson, S., Hansman, R. L., Bam, W., Bock, C., & Swarzenski, P. W. (2020). Exploring new frontiers in marine radioisotope tracing–adapting to new opportunities and challenges. *Frontiers in Marine Science*, *7*, 406.

Dalencourt, C., Chabane, M. N., Tremblay-Cantin, J.-C., & Larivière, D. (2020). A rapid sequential chromatographic separation of U- and Th-decay series radionuclides in water samples. *Talanta*, *207*, 120282. https://doi.org/https://doi.org/10.1016/j.talanta.2019.120282

Das, R., & Choudhury, I. (2013). Waste management in mining industry. *Indian Journal of Scientific Research*, 139-142.

Davis, M. J. (2004). *Measurement uncertainties and minimum detectable concentrations for the in situ NaI gamma spectroscopy systems used at the Fernald site* (ANL/EAD/TM/04-02). http://www.osti.gov/servlets/purl/828775-l55fpt/native/

Dogan, I., Ozyigit, I. I., Kidiraliyeva, B., Cekirov, K., Kurmanbekova, G., Ucar, B., Saykieva, N., Hocaoglu-Ozyigit, A., Yalcin, I. E., Severoglu, Z., & Solak, A. O. (2021). Assessment of pollution at the former uranium waste dumpsite near kaji-Say Village/Kyrgyzstan: a genetic and physiological investigation. *Journal of Radiation Research and Applied Sciences*, *14*(1), 280-294. https://doi.org/https://doi.org/10.1080/16878507.2021.1957397

Duff, M. C., Coughlin, J. U., & Hunter, D. B. (2002). Uranium co-precipitation with iron oxide minerals. *Geochimica et Cosmochimica Acta*, *66*(20), 3533-3547. https://doi.org/https://doi.org/10.1016/S0016-7037(02)00953-5

Durand, J. F. (2012). The impact of gold mining on the Witwatersrand on the rivers and karst system of Gauteng and North West Province, South Africa. *Journal of Arican Earth Sciences*, 24-43.

Durrheim, R. J. (2010). Mitigating the risk of rockbursts in the deep hard rock mines of South Africa: 100 years of research. *Extracting the Science: a century of mining research*, 156-171.

El-Sharkawy, A. M. (2018). $^{234}U/^{238}U$ activity ratios in groundwaters from two aquifers in Saudi Arabia, and correlation with water chemistry. *Journal of Radiation Research and Applied Sciences*, *11*(4), 368-372. https://doi.org/https://doi.org/10.1016/j.jrras.2018.07.005

Els, B. (1998). The question of alluvial fans in the auriferous Archaean and Proterozoic succession of South Africa. *South African Journal of Geology*, *101*(1), 17-25.

Ford, M. A. (1993). Uranium in South Africa. *Journal of The South African Institute of Mining and Metallurgy*, 37-58.

Frimmel, H., Groves, D., Kirk, J., Ruiz, J., Chesley, J., & Minter, W. (2005). The formation and preservation of the Witwatersrand goldfields, the world's largest gold province. *Economic Geology*, *100*, 769-797.

Frimmel, H., & Minter, W. (2002). Recent developments concerning the geological history and genesis of the Witwatersrand gold deposits, South Africa. *SPECIAL PUBLICATION-SOCIETY OF ECONOMIC GEOLOGISTS*, *9*, 17-46.

Frimmel, H. E. (2018). Episodic concentration of gold to ore grade through Earth's history. *Earth-Science Reviews*, *180*, 148-158. https://doi.org/https://doi.org/10.1016/j.earscirev.2018.03.011

Fuchs, S., Schumann, D., Martin, R. F., & Couillard, M. (2021). The extensive hydrocarbon-mediated fixation of hydrothermal gold in the Witwatersrand Basin, South Africa. *Ore Geology Reviews*, *138*, 104313. https://doi.org/https://doi.org/10.1016/j.oregeorev.2021.104313

Fuchs, S., Williams-Jones, A. E., & Przybylowicz, W. J. (2016). The origin of the gold and uranium ores of the Black Reef Formation, Transvaal Supergroup, South Africa. *Ore Geology Reviews*, *72*, 149-164. https://doi.org/https://doi.org/10.1016/j.oregeorev.2015.07.010

Funke, J. W. (1990). *The water requirements and pollution potential of South African gold and uranium mines*.

Garner, J., Cairns, J., & Read, D. (2015). NORM in the East Midlands' oil and gas producing region of the UK. *Journal of Environmental Radioactivity*, *150*, 49-56. https://doi.org/https://doi.org/10.1016/j.jenvrad.2015.07.016

Gascoyne, M. (1992). The geochemistry of the actinides and their daughters. In *Uranium-Series Disequilibrium: Applications to Earth, Marine, and Environmental Sciences (second ed.)* (pp. 3458). Clarendon Press.

Geipel, G., & Bernhard, G. (2008). Uranium Speciation - from mineral phases to mineral waters. In *Uranium, Mining and Hydrogeology* (pp. 599-601). Springer.

Guillaumont, R., Fanghänel, T., Fuger, J., Grenthe, I., Neck, V., Palmer, D., & Rand, M. (2003). *Update on the chemical thermodynamics of uranium, neptunium, plutonium, americium and technetium*. Elsevier Science Publishers.

Guirguis, L. A., Farag, N. M., & Salim, A. K. (2015). Accurate fast method with high chemical yield for determination of uranium isotopes (^{234}U, ^{235}U, ^{238}U) in granitic samples using alpha spectroscopy. *Nuclear Instruments and Methods in Physics Research Section A: Accelerators, Spectrometers, Detectors and Associated Equipment*, *777*, 211-217. https://doi.org/https://doi.org/10.1016/j.nima.2015.01.016

Guy, B. M., Ono, S., Gutzmer, J., Kaufman, A. J., Lin, Y., Fogel, M. L., & Beukes, N. J. (2012). A multiple sulfur and organic carbon isotope record from non-conglomeratic sedimentary rocks of the Mesoarchean Witwatersrand Supergroup, South Africa. *Precambrian Research*, *216-219*, 208-231. https://doi.org/https://doi.org/10.1016/j.precamres.2012.06.018

Hansen, R. N. (2015). Contaminant leaching from gold mining tailings dams in the Witwatersrand Basin, South Africa: A new geochemical modelling approach. *Applied Geochemistry*, *61*, 217-223. https://doi.org/https://doi.org/10.1016/j.apgeochem.2015.06.001

Henning, C., Tsushima, S., Brendler, V., Ikeda, A., Scheinost, A., & Bernhard, G. (2008). Coordination of U(IV) and U(VI) sulfate hydrate in aqueous solution. In *Uranium, Mining and Hydrogeology* (pp. 603-612). Springer.

Hindman, F. D. (1983). Neodymium fluoride mounting for .alpha. spectrometric determination of uranium, plutonium, and americium. *Analytical Chemistry*, *55*(14), 2460-2461. https://doi.org/10.1021/ac00264a068

Hodgson, K., & Manus, L. (2006). A drinking water quality framework for South Africa. *Water SA*, *32*. https://doi.org/10.4314/wsa.v32i5.47853

IAEA, I. (2003). Guidelines for radioelement mapping using gamma ray spectrometry data. *Vienna: International Atomic Energy Agency*.

Janisch, P. (1986). Gold in South Africa. *Journal of The South African Institute of Mining and Metallurgy*, 273-316.

Jia, G., Belli, M., Sansone, U., Rosamilia, S., Ocone, R., & Gaudino, S. (2002). Determination of uranium isotopes in environmental samples by alpha-spectrometry. *Journal of Radioanalytical and Nuclear Chemistry*, *253*(3), 395-406. https://doi.org/https://doi.org/10.1023/a:1020413302019

Jolley, S. J., Freeman, S. R., Barnicoat, A. C., Phillips, G. M., Knipe, R. J., Pather, A., Fox, N. P. C., Strydom, D., Birch, M. T. G., Henderson, I. H. C., & Rowland, T. W. (2004). Structural controls on Witwatersrand gold mineralisation. *Journal of Structural Geology*, *26*(6), 1067-1086. https://doi.org/https://doi.org/10.1016/j.jsg.2003.11.011

Jurečič, S., Benedik, L., Planinšek, P., Nečemer, M., Kump, P., & Pihlar, B. (2014). Analysis of uranium in the insoluble residues after decomposition of soil samples by various techniques. *Applied Radiation and Isotopes*, *87*, 61-65. https://doi.org/https://doi.org/10.1016/j.apradiso.2013.11.077

Kanai, Y., & Sakamaki, Y. (1994). Uranium redistribution implied by 234U/238U disequilibrium study on apatite-bearing sedimentary rocks at Nakamaruke district,

central Japan. *Applied Geochemistry*, *9*(5), 547-552. https://doi.org/https://doi.org/10.1016/0883-2927(94)90016-7

Killeen, P. G., Mwenifumbo, C. J., & Ford, K. L. (2015). 11.14 - Tools and Techniques: Radiometric Methods. In G. Schubert (Ed.), *Treatise on Geophysics (Second Edition)* (pp. 447-524). Elsevier. https://doi.org/https://doi.org/10.1016/B978-0-444-53802-4.00209-8

Koppel, D. J., Kho, F., Hastings, A., Crouch, D., MacIntosh, A., Cresswell, T., & Higgins, S. (2022). Current understanding and research needs for ecological risk assessments of naturally occurring radioactive materials (NORM) in subsea oil and gas pipelines. *Journal of Environmental Radioactivity*, *241*, 106774. https://doi.org/https://doi.org/10.1016/j.jenvrad.2021.106774

Kositcin, N., & Krapež, B. (2004). Relationship between detrital zircon age-spectra and the tectonic evolution of the Late Archaean Witwatersrand Basin, South Africa. *Precambrian Research*, *129*(1), 141-168. https://doi.org/https://doi.org/10.1016/j.precamres.2003.10.011

Kossoff, D., Dubbin, W. E., Alfredsson, M., Edwards, S. J., Macklin, M. G., & Hudson-Edwards, K. A. (2014). Mine tailings dams: Characteristics, failure, environmental impacts, and remediation. *Applied Geochemistry*, *51*, 229-245. https://doi.org/https://doi.org/10.1016/j.apgeochem.2014.09.010

Krachler, R., Krachler, R., Gúlce, F., Keppler, B., & Wallner, G. (2018). Uranium concentrations in sediments pore waters of Lake Neusiedl, Austria. *Science of The Total Environment*, 981-988.

L'Annunziata, M. F. (2007). *Radioactivity: Introduction and History*. Elsevier.

Lapworth, D. J., Brauns, B., Chattopadhyay, S., Gooddy, D. C., Loveless, S. E., MacDonald, A. M., McKenzie, A. A., Muddu, S., & Nara, S. N. V. (2021). Elevated uranium in drinking water sources in basement aquifers of southern India. *Applied Geochemistry*, *133*, 105092. https://doi.org/https://doi.org/10.1016/j.apgeochem.2021.105092

Lau, M. C. Y., Kieft, T. L., Kuloyo, O., Linage-Alvarez, B., van Heerden, E., Lindsay, M. R., Magnabosco, C., Wang, W., Wiggins, J. B., Guo, L., Perlman, D. H., Kyin, S., Shwe, H. H., Harris, R. L., Oh, Y., Yi, M. J., Purtschert, R., Slater, G. F., Ono, S., . . . Onstott, T. C. (2016). An oligotrophic deep-subsurface community dependent on syntrophy is dominated by sulfur-driven autotrophic denitrifiers. *Proceedings of the National Academy of Sciences*, *113*(49), E7927-E7936. https://doi.org/10.1073/pnas.1612244113

Li, L., Wei, S., Sherwood Lollar, B., Wing, B., Bui, T. H., Ono, S., Lau Vetter, M. C. Y., Onstott, T. C., Kieft, T. L., Borgonie, G., Linage-Alvarez, B., Kuloyo, O., & van

Heerden, E. (2022). In situ oxidation of sulfide minerals supports widespread sulfate reducing bacteria in the deep subsurface of the Witwatersrand Basin (South Africa): Insights from multiple sulfur and oxygen isotopes. *Earth and Planetary Science Letters*, *577*, 117247. https://doi.org/https://doi.org/10.1016/j.epsl.2021.117247

Li, T., Cao, Y., Li, B., & Dai, R. (2021). The biological effects of radiation-induced liver damage and its natural protective medicine. *Progress in Biophysics and Molecular Biology*, *167*, 87-95. https://doi.org/https://doi.org/10.1016/j.pbiomolbio.2021.06.012

Li, Z., Hadioui, M., & Wilkinson, K. J. (2019). Conditions affecting the release of thorium and uranium from the tailings of a niobium mine. *Environmental Pollution*, *247*, 206-215. https://doi.org/https://doi.org/10.1016/j.envpol.2018.12.042

Lohrabian, V., Kamali-Asl, A., Harvani, H. G., Hosseini Aghdam, S. R., Arabi, H., & Zaidi, H. (2021). Comparison of the X-ray tube spectrum measurement using BGO, NaI, LYSO, and HPGe detectors in a preclinical mini-CT scanner: Monte Carlo simulation and practical experiment. *Radiation Physics and Chemistry*, *189*, 109666. https://doi.org/https://doi.org/10.1016/j.radphyschem.2021.109666

Lysandrou, M., & Pashalidis, I. (2008). Uranium chemistry in stack solutions and leachates of phosphogypsum disposed at a coastal area in Cyprus. *Journal of Environmental Radioactivity*, 359-366.

Maes, S., Zhuang, W.-Q., Rabaey, K., Alvarez-Cohen, L., & Hennebel, T. (2017). Concomitant Leaching and Electrochemical Extraction of Rare Earth Elements from Monazite. *Environmental Science & Technology*, *51*(3), 1654-1661. https://doi.org/10.1021/acs.est.6b03675

Magnabosco, C., Timmers, P. H., Lau, M. C., Borgonie, G., Linage-Alvarez, B., Kuloyo, O., Alleva, R., Kieft, T. L., Slater, G., & van Heerden, E. (2018). Fluctuations in populations of subsurface methane oxidizers in coordination with changes in electron acceptor availability. *FEMS microbiology ecology*, *94*(7), fiy089.

Marais, L., & Nel, E. (2016). The dangers of growing on gold: Lessons for mine downscaling from the Free State Goldfields, South Africa. *Local Economy*, *31*(1-2), 282-298.

McLean, C. (1994). The uranium industry of South Africa. *The Journal of The South African Institute of Mining and Metallurgy*, 113-122.

Mirion. (2019). *High-Resolution Gamma-Ray Spectroscopy with HPGe Detectors*. https://www.mirion.com/learning-center/lab-experiments/high-resolution-gamma-spectroscopy-with-hpge-detectors-lab-experiments

Moll, H., Reich, T., Hennig, C., Rossberg, A., Szabo, Z., & Grenthe, I. (2000). Solution coordination chemistry of uranium in the binary UO_2^{2+}-$SO_4^{2-}$and the ternary UO_2^{2+}-SO_4^{2-}-OH^-system. *Radiochimica Acta*, *88*(9-11), 559-566.

Montgomery, D. (1998). Establishing the traceability of radioactivity standards to the National Institute of Standards and Technology (NIST). *Journal of Radioanalytical and Nuclear Chemistry*, *233*(1-2), 21-24. https://doi.org/10.1007/bf02389641

Njinga, R. L., & Tshivhase, V. M. (2017). The impact of mine tailings on the Witwatersrand and the surrounding water bodies in Gauteng Province, South Africa. *Mine Water and the Environment*, *36*(4), 638-645.

Nwaila, G. T., Ghorbani, Y., Zhang, S. E., Frimmel, H. E., Tolmay, L. C. K., Rose, D. H., Nwaila, P. C., & Bourdeau, J. E. (2021). Valorisation of mine waste - Part I: Characteristics of, and sampling methodology for, consolidated mineralised tailings by using Witwatersrand gold mines (South Africa) as an example. *Journal of Environmental Management*, *295*, 113013. https://doi.org/https://doi.org/10.1016/j.jenvman.2021.113013

Olivares, D. M. M., Guevara, M. M., & Velasco, F. G. (2017). Determination of the HPGe detector efficiency in measurements of radioactivity in extended environmental samples. *Applied Radiation and Isotopes*, *130*, 34-42.

Onstott, T. C., Lin, L. H., Davidson, M., Mislowack, B., Borcsik, M., Hall, J., Slater, G., Ward, J., Lollar, B. S., Lippmann-Pipke, J., Boice, E., Pratt, L. M., Pfiffner, S., Moser, D., Gihring, T., Kieft, T. L., Phelps, T. J., Vanheerden, E., Litthaur, D., . . . Southam, G. (2006). The Origin and Age of Biogeochemical Trends in Deep Fracture Water of the Witwatersrand Basin, South Africa. *Geomicrobiology Journal*, *23*(6), 369-414. https://doi.org/10.1080/01490450600875688

Papadopoulos, A., Christofides, G., Koroneos, A., Stoulos, S., & Papastefanou, C. (2013). Radioactive secular equilibrium in ^{238}U and ^{232}Th series in granitoids from Greece. *Applied Radiation and Isotopes*, 95-104.

Papanicolaou, F., Antoniou, S., & Pashalidis, I. (2010). Redox chemistry of sulphate and uranium in a phosphogypsum tailings dump. *Journal of Environmental Radioactivity*, *101*(8), 601-605.

Pavan, M., Raja, V., & Barron, A. (2019). *Principles of Gamma-ray Spectrometry and Applications in Nuclear Forensics*. https://chem.libretexts.org/Bookshelves/Analytical_Chemistry/Book%3A_Physical_Methods_in_Chemistry_and_Nano_Science_(Barron)/01%3A_Elemental_Analysis/1.17%3A_Principles_of_Gamma-ray_Spectroscopy_and_Applications_in_Nuclear_Forensics

Payne, T., Brendler, V., Comarmond, M., & Nebelung, C. (2011). Assessment of surface area normalisation for interpreting distribution coefficients (Kd) for uranium sorption *Journal of Environmental Radioactivity*, 888-895.

Perold, P. (2013). *New Technological Applications in deep-level gold mining* (R105/2013).

Pham, L. T. (2021). A high resolution edge detector for interpreting potential field data: A case study from the Witwatersrand basin, South Africa. *Journal of African Earth Sciences*, *178*, 104190. https://doi.org/https://doi.org/10.1016/j.jafrearsci.2021.104190

Phillips, G. (1987). Metamorphism of the Witwatersrand gold fields: conditions during peak metamorphism. *Journal of Metamorphic Geology*, *5*(3), 307-322.

Phrommavanh, V., Vercouter, T., Descostes, M., Beaucaire, C., & Gaudet, J. (2008). Speciation of Uranium in a Polluted Site: a TRLFS study. In *Uranium, Mining and Hydrogeology* (pp. 621-622). Springer.

Prabhu, S. P., Gupta, P., & Rao, D. (2016). Use of solid extraction chromatography for determination of uranium in sea water and brine. *Desalination and Water Treatment*, *57*, 1-5. https://doi.org/10.1080/19443994.2016.1139104

Prozorova, I. V., Ghal-Eh, N., Bedenko, S. V., Popov, Y. A., Prozorov, A. A., & Vega-Carrillo, H. R. (2021). Characterizing the coaxial HPGe detector using Monte Carlo simulations and evolutionary algorithms. *Applied Radiation and Isotopes*, *174*, 109748. https://doi.org/https://doi.org/10.1016/j.apradiso.2021.109748

Puphal, K. W., & Olsen, D. R. (1972). Electrodeposition of .alpha.-emitting nuclides from a mixed oxalate-chloride electrolyte. *Analytical Chemistry*, *44*(2), 284-289. https://doi.org/10.1021/ac60310a014

Riemer, K. L., & Durrheim, R. J. (2012). Mining seismicity in the Witwatersrand Basin: monitoring, mechanisms and mitigation strategies in perspective. *Journal of Rock Mechanics and Geotechnical Engineering*, *4*(3), 228-249. https://doi.org/https://doi.org/10.3724/SP.J.1235.2012.00228

Robb, L., & Robb, V. (1998). Environmental impact of Witwatersrand gold mining. In *The Mineral Resources of South Africa* (pp. 14-16). Council for Geoscience.

Sai, K. V., Rao, K. M., Rajasekhar, E., Rao, D. R., Seetharaman, D., & Kamisetti, V. (2022). Precise conversion electron intensities of low energy gamma transitions for efficiency calibration of electron detectors. *Applied Radiation and Isotopes*, *189*, 110410. https://doi.org/https://doi.org/10.1016/j.apradiso.2022.110410

Salazar, S., Castillo, L. A., & Montes, L. (2021). Evaluation of naturally occurring radioactive materials (NORM) in the soil, in a potential area for unconventional reservoirs in the

Rancheria Sub-Basin. *Chemosphere*, *283*, 131098. https://doi.org/https://doi.org/10.1016/j.chemosphere.2021.131098

Schonfield, S., Winde, F., Albrecht, C., Kielkowski, D., Liefferink, M., Patel, M., Sewram, V., Whitaker, C., & Schüz, J. (2014). Health effects in populations living around the uraniferous gold mine tailings in South Africa: Gaps and opportunitites for research. *International Journal of Cancer Epidemiology, Gaps and opportunities for research* 628-632.

Selvig, L. K., Inn, K. G. W., Outola, I. M. J., Kurosaki, H., & Lee, K. A. (2005). Dissolution of resistate minerals containing uranium andthorium: Environmental implications. *Journal of Radioanalytical and Nuclear Chemistry*, *263*(2), 341-348. https://doi.org/10.1007/s10967-005-0060-y

Shazly, A., Kany, A., El Samman, H., & El-Mongy, S. (2012). Nondestructive compton suppression technique for verification of the (%E) values in natural ore samples. *Journal of Nuclear & Radiation Physics*, 41-53.

Shukla, A., Parmar, P., Goswami, D., Patel, B., & Saraf, M. (2020). Characterization of novel thorium tolerant Ochrobactrum intermedium AM7 in consort with assessing its EPS-Thorium binding. *Journal of Hazardous Materials*, *388*, 122047. https://doi.org/https://doi.org/10.1016/j.jhazmat.2020.122047

Sill, C. W., & Williams, R. L. (1981). Preparation of actinides for .alpha. spectrometry without electrodeposition. *Analytical Chemistry*, *53*(3), 412-415. https://doi.org/10.1021/ac00226a008

Su, J., Gao, Y., Ni, S., Xu, R., & Sun, X. (2021). A safer and cleaner process for recovering thorium and rare earth elements from radioactive waste residue. *Journal of Hazardous Materials*, *406*, 124654. https://doi.org/https://doi.org/10.1016/j.jhazmat.2020.124654

Tucker, R. F., Viljoen, R. P., & Viljoen, M. J. (2016). A review of the Witwatersrand Basin–The world's greatest goldfield. *Episodes*, *39*(2), 105-133.

Vadja, N. (2012). Alpha Spectrometry. *Handbook of Radioactivity Analysis*, 364.

Vajda, N., Pöllänen, R., Martin, P., & Kim, C.-K. (2020). Chapter 5 - Alpha spectrometry. In M. F. L'Annunziata (Ed.), *Handbook of Radioactivity Analysis (Fourth Edition)* (pp. 493-573). Academic Press. https://doi.org/https://doi.org/10.1016/B978-0-12-814397-1.00005-4

Valković, V. (2019). Chapter 4 - Measurements of radioactivity. In V. Valković (Ed.), *Radioactivity in the Environment (Second Edition)* (pp. 123-280). Elsevier. https://doi.org/https://doi.org/10.1016/B978-0-444-64146-5.00004-5

Van Eeden, E., Liefferink, M., & Durand, J. (2009). Legal issues concerning mine closure and social responsibility on the West Rand. *The Journal for Transdisciplinary Research in Southern Africa*, 51-71.

Veale, M. (2009). *Charge Transport and low Temperature Phenomena in Single Crystal CdZnTe*

Veerasamy, N., Kasar, S., Murugan, R., Inoue, K., Natarajan, T., Chand Ramola, R., Fukushi, M., & Kumar Sahoo, S. (2023). $^{234}U/^{238}U$ disequilibrium and $^{235}U/^{238}U$ ratios measured using MC-ICP-MS in natural high background radiation area soils to understand the fate of uranium. *Chemosphere*, *323*, 138217. https://doi.org/https://doi.org/10.1016/j.chemosphere.2023.138217

Venter, I. (2001). South African mining sector facing radiation challenge. *Mining Weekly*, *7*(43), 2-3.

Vetesnik, A., Semelová, M., Stamberg, K., & Vopálka, D. (2008). Uranium(VI)Sulfate Complexation as a Function of Temperature and Ionic Strength Studied by TRLFS. In *Uranium, Mining and Hydrogeology* (pp. 621-630). Spinger.

Vukanac, I., Šešlak, B., Kandić, A., Čeliković, I., Nikolić, N. M., Milanović, T., Obradović, Z., & Đurašević, M. (2022). A comparison of alpha-particle and gamma-ray spectrometry methods for determination of ^{235}U, ^{238}U and ^{226}Ra activity concentration in samples of coal, slag and fly-ash. *Radiation Physics and Chemistry*, *193*, 109933. https://doi.org/https://doi.org/10.1016/j.radphyschem.2021.109933

Walencik-Łata, A., Kozłowska, B., & Przylibski, T. A. (2021). Hydrochemical behaviour of dissolved uranium in selected groundwaters of the Kłodzko Valley (SW Poland) and its application possibilities as an environmental tracer. *Chemosphere*, *267*, 128911. https://doi.org/https://doi.org/10.1016/j.chemosphere.2020.128911

Wang, Z., Brown, A. T., Tan, K., Chabal, Y. J., & Balkus, K. J. (2018). Selective Extraction of Thorium from Rare Earth Elements Using Wrinkled Mesoporous Carbon. *Journal of the American Chemical Society*, *140*(44), 14735-14739. https://doi.org/10.1021/jacs.8b07610

Winde, F. (2001). Fluvial processes and uranium transport-pitfalls from the Wismut region (Germany) and the Klerksdorp gold field (South Africa). Proceedings of the Fourth International Conference of the Society of South African Geographers, Goudino Spa.

Winde, F., & de Villiers, A. (2002). The nature and extent of uranium contamination from tailings dams in the Witwatersrand gold mining area-South Africa. In *Uranium in the Aquatic Environment* (pp. 889-897). Heidelberg.

Winde, F., & de Villiers, A. B. (2002). Uranium contamination of streams by tailings deposits—case studies in the Witwatersrand gold mining area (South Africa). Uranium in the Aquatic Environment: Proceedings of the International Conference Uranium Mining and Hydrogeology III and the International Mine Water Association Symposium Freiberg, Germany, 15-21 September 2002,

Winde, F., Erasmus, E., & Geipel, G. (2017). Uranium contaminated drinking water linked to leukaemia—Revisiting a case study from South Africa taking alternative exposure pathways into account. *Science of The Total Environment*, *574*, 400-421. https://doi.org/https://doi.org/10.1016/j.scitotenv.2016.09.035

Winde, F., Hoffmann, E., Espina, C., & Schüz, J. (2019). Mapping and modelling human exposure to uraniferous mine waste using a GIS-supported virtual geographic environment. *Journal of Geochemical Exploration*, 167-180.

Winde, F., & Sandham, L. A. (2004). Uranium pollution of South African streams - An overview of the situation in gold mining areas of the Witwatersrand. *GeoJournal*, 131-149.

Winde, F., & van der Walt, I. J. (2004). The significance of groundwater-stream interactions and fluctuating stream chemistry on waterborne uranium contamination of streams - a case study from a gold mining site in South Africa. *Journal of Hydrology*, 178-196.

Wolkersdorfer, C., Mugova, E., Daga, V. S., Charvet, P., & Vitule, J. R. S. (2021). Effects of Mining on Surface Water—Case Studies. In *Reference Module in Earth Systems and Environmental Sciences*. Elsevier. https://doi.org/https://doi.org/10.1016/B978-0-12-819166-8.00085-2

Xhixha, G., Baldoncini, M., Callegari, I., Colonna, T., Hasani, F., Mantovani, F., Shala, F., Strati, V., & Xhixha Kaçeli, M. (2015). A century of oil and gas exploration in Albania: Assessment of Naturally Occurring Radioactive Materials (NORMs). *Chemosphere*, *139*, 30-39. https://doi.org/https://doi.org/10.1016/j.chemosphere.2015.05.018

Yu, L., Lin, Z., Cheng, X., Chu, J., Li, X., Chen, C., Zhu, T., Li, W., Lin, W., & Tang, W. (2022). Thorium inhibits human respiratory chain complex IV (cytochrome c oxidase). *Journal of Hazardous Materials*, *424*, 127546. https://doi.org/https://doi.org/10.1016/j.jhazmat.2021.127546

Yücel, H., Çetiner, M. A., & Demirel, H. (1998). Use of the 1001keV peak of ^{234m}Pa daughter of ^{238}U in measurement of uranium concentration by HPGe gamma-ray spectrometry. *Nuclear Instruments and Methods in Physics Research Section A: Accelerators, Spectrometers, Detectors and Associated Equipment*, *413*(1), 74-82. https://doi.org/https://doi.org/10.1016/S0168-9002(98)00562-2

Zielinski, R., Simmons, K., & Orem, W. (2000). Use of ^{234}U and ^{238}U isotopes to identify fertilizer-derived uranium in the Florida Everglades. *Applied Geochemistry*, 369-383.

NWU®
NORTH-WEST UNIVERSITY
NOORDWES-UNIVERSITEIT
YUNIBESITI YA BOKONE BOPHIRIMA

Private Bag X1290, Potchefstroom
South Africa 2520
Tel: 018 299-1111/2222
Fax: 018 299-4910
Web: http://www.nwu.ac.za
Senate Committee for Research Ethics
Tel: 018 299-4849
Email: nkosinathi.machine@nwu.ac.za

ETHICS APPROVAL LETTER OF STUDY

Based on the review by the **Faculty of Natural and Agricultural Sciences Ethics Committee (FNASREC)**, the Committee hereby clears your study as no ethical risk. This implies that the FNASREC grants permission that, provided the general conditions specified below are met, the study may be initiated, using the ethics number below.

Study title: Determining Uranium activity distribution in water and sediment around gold mining regions
Study Leader/Supervisor: Dr A Ocwelwang
Student: P Mashamaite

Ethics number: N | W | U | - | 0 | 1 | 2 5 6 - 2 2 - A 9
Institution Study Number Year Status

Status: S = Submission; R = Re-Submission; P = Provisional Authorisation; A = Authorisation

Application type: Single **Risk Category:** **No Risk**

Commencement date: 25/06/2022
Expiry date: 30/08/2023

General conditions:
The following general terms and conditions apply:

- *The commencement date indicates the date when the study may be started.*
- *In the interest of ethical responsibility, the NWU-SCRE and FNASREC reserves the right to:*
  - *request access to any information or data at any time during the course or after completion of the study;*
  - *to ask further questions, seek additional information, require further modification or monitor the conduct of your research or the informed consent process;*
  - *withdraw or postpone approval if:*
    - *any unethical principles or practices of the study are revealed or suspected;*
    - *it becomes apparent that any relevant information was withheld from the FNASREC or that information has been false or misrepresented;*
    - *submission of the annual (or otherwise stipulated) monitoring report, the required amendments, or reporting of adverse events or incidents was not done in a timely manner and accurately; and / or*
    - *new institutional rules, national legislation or international conventions deem it necessary.*
- *FNASREC can be contacted for further information or any report templates via Roelof.Burger@nwu.ac.za 018 299 4269*

The FNASREC would like to remain at your service as scientist and researcher, and wishes you well with your study. Please do not hesitate to contact the FNASREC or the NWU-SCRE for any further enquiries or requests for assistance.

Yours sincerely,

Prof Roelof Burger
Chairperson Faculty of Natural and Agricultural Sciences Ethics Committee (FNASREC)

File reference: 9.1.5.4.2

Page 1 of 1